

The Neoproterozoic Hüttenberg $\delta^{13}\text{C}$ anomaly: Genesis and global implications

Huan Cui^{a,b,*}, Alan J. Kaufman^b, Yongbo Peng^c, Xiao-Ming Liu^d, Rebecca E. Plummer^{b,1}, Elizabeth I. Lee^{b,2}

^a NASA Astrobiology Institute, Department of Geoscience, University of Wisconsin–Madison, Madison, WI 53706, USA

^b Department of Geology and Earth System Science Interdisciplinary Center, University of Maryland, College Park, MD 20742, USA

^c Department of Geology and Geophysics, Louisiana State University, Baton Rouge, LA 70803, USA

^d Department of Geological Sciences, University of North Carolina, Chapel Hill, NC 27599, USA

ARTICLE INFO

Keywords:
Hüttenberg anomaly
Neoproterozoic
Chemostratigraphy
Carbon cycle
Positive excursion
Sulfur isotopes
Namibia

ABSTRACT

The Neoproterozoic Hüttenberg Formation in northeastern Namibia records a remarkable $\delta^{13}\text{C}_{\text{carb}}$ positive excursion with a sustained plateau of values up to +12‰ (i.e., the Hüttenberg anomaly). High-resolution chemostratigraphic analyses of drill core samples spanning the upper Elandshoek and Hüttenberg formations reveal multiple new observations: (1) overall high but oscillatory $\delta^{13}\text{C}_{\text{carb}}$ values; (2) $\delta^{18}\text{O}_{\text{carb}}$ values ranging from −8‰ to −2‰; (3) significant enrichment of ^{13}C in organic carbon and a broad co-variation between $\delta^{13}\text{C}_{\text{carb}}$ and $\delta^{13}\text{C}_{\text{org}}$; (4) a profound negative excursion in $\delta^{34}\text{S}_{\text{pyrite}}$ from +30‰ to −10‰; (5) an overall inverse $\delta^{13}\text{C}$ – $\delta^{34}\text{S}$ relationship; and (6) $^{87}\text{Sr}/^{86}\text{Sr}$ values down to 0.7074 in limestone samples. The new data suggest that the Hüttenberg anomaly records dynamic fluctuations in marine redox conditions, which may include an oxygenation event during the height of the $\delta^{13}\text{C}_{\text{carb}}$ positive excursion and a deoxygenation event at its termination. The $\delta^{34}\text{S}_{\text{pyrite}}$ negative excursion suggests the buildup of the marine sulfate reservoir, likely due to enhanced pyrite oxidation during the oxygenation event. The $\delta^{34}\text{S}_{\text{pyrite}}$ increase at the end of the Hüttenberg anomaly may result from a seawater sulfate concentration drawdown towards pre-anomaly conditions. On one hand, the Hüttenberg anomaly may reflect restricted basin signals that are deviated from the Ediacaran open ocean; on the other hand, the Ediacaran Hüttenberg anomaly, together with the Cryogenian $\delta^{13}\text{C}_{\text{carb}}$ positive excursions, suggests a stepwise pattern of the Neoproterozoic Oxygenation Event. Both local and global environmental factors may have contributed to the Hüttenberg anomaly. The Hüttenberg anomaly therefore represents a local enhancement of global oxygenation signals. Our data support the emerging view that the Neoproterozoic Oxygenation Event may have facilitated the evolution of early life at that time.

1. Introduction

The global carbon cycle plays an essential role as both a driver and a monitor of redox processes in the oceans and atmosphere (Hayes and Waldbauer, 2006). The deep-time history of the carbon cycle is preserved in the sedimentary record of carbonates and co-existing organic matter. By analyzing stratigraphic patterns of carbon isotope ratios in carbonates ($\delta^{13}\text{C}_{\text{carb}}$) and organic matter ($\delta^{13}\text{C}_{\text{org}}$), the evolution of the carbon cycle through time can be reconstructed (Knoll et al., 1986; Kaufman et al., 1997; Saltzman and Thomas, 2012), which in turn can be related to environmental, climatic, and biological events in Earth history.

Significant efforts have been focused on the oscillatory pattern of $\delta^{13}\text{C}_{\text{carb}}$ variations through the Proterozoic Eon, with strong negative perturbations intimately coupled with ice ages (Kaufman et al., 1997; Hoffman et al., 1998b; Halverson et al., 2002; Halverson et al., 2005; Halverson et al., 2010; Halverson and Shields-Zhou, 2011; Shields-Zhou et al., 2012), or the enigmatic Shuram Excursion of the Ediacaran Period (Fike et al., 2006; Jiang et al., 2007; McFadden et al., 2008; Grotzinger et al., 2011; Cui et al., 2015; Husson et al., 2015; Cui, 2017; Cui et al., 2017; Verdel et al., 2011). However, less attention has been paid to the extreme positive $\delta^{13}\text{C}_{\text{carb}}$ excursions, which have been interpreted as periods of extreme productivity and burial of organic carbon in sedimentary reservoirs (Knoll et al., 1986; Kaufman et al.,

* Corresponding author at: NASA Astrobiology Institute, Department of Geoscience, University of Wisconsin–Madison, Madison, WI 53706, USA.
E-mail address: Huan.Cui@wisc.edu (H. Cui).

¹ Present address: Hydrology and Remote Sensing Laboratory, Beltsville Agricultural Research Center, US Department of Agriculture, Beltsville, MD 20705, USA.

² Present address: Department of Geology, University at Buffalo, The State University of New York, Buffalo, NY 14260, USA.

Table 1Compilation of the Neoproterozoic $\delta^{13}\text{C}_{\text{carb}}$ positive anomalies.

| Period | Strata | Chemostratigraphy | References |
|----------------|--|---|---|
| Ediacaran | Dengying Formation, South China | $\delta^{13}\text{C}$ up to ca. +6‰ $^{87}\text{Sr}/^{86}\text{Sr}$: 0.7084 | (Jiang et al., 2007; Zhou and Xiao, 2007; Zhu et al., 2007; Cui et al., 2016b) |
| Ediacaran | Doushantuo Formation, South China | $\delta^{13}\text{C}$ up to ca. +8‰ $^{87}\text{Sr}/^{86}\text{Sr}$: 0.7080–0.7090 | (Jiang et al., 2007; Zhou and Xiao, 2007; Zhu et al., 2007; McFadden et al., 2008; Sawaki et al., 2010; Tahata et al., 2013; Cui et al., 2016b; Gao et al., 2018) |
| Neoproterozoic | Multiple strata in Svalbard and East Greenland | $\delta^{13}\text{C}$ up to ca. +10‰ | (Knoll et al., 1986; Derry et al., 1989; Kaufman et al., 1997; Halverson et al., 2004; Halverson et al., 2005; Halverson et al., 2007) |
| Cryogenian | Keele Formation, Canada | $\delta^{13}\text{C}$ up to ca. +10‰ $^{87}\text{Sr}/^{86}\text{Sr}$: 0.7071–0.7073 | (Narbonne et al., 1994; Kaufman et al., 1997) |
| Cryogenian | Etina Formation, Australia | $\delta^{13}\text{C}$ up to ca. +10‰ $^{87}\text{Sr}/^{86}\text{Sr}$: 0.7076–0.7078 | (Walter et al., 2000; McKirdy et al., 2001; Swanson-Hysell et al., 2010; Rose et al., 2012) |
| Cryogenian | Tayshir Formation, Mongolia | $\delta^{13}\text{C}$ up to ca. +12‰ $^{87}\text{Sr}/^{86}\text{Sr}$: 0.7072–0.7074 | (Brasier et al., 1996a; Brasier et al., 1996b; Shields et al., 1997; Shields et al., 2002; Macdonald et al., 2009; Bold et al., 2016) |
| Ediacaran | Hüttenberg Formation, Namibia | $\delta^{13}\text{C}$ up to ca. +12‰ $^{87}\text{Sr}/^{86}\text{Sr}$: 0.7074 | (Kaufman et al., 1991; Kaufman et al., 2009) and this study |
| Neoproterozoic | Una Group, Brazil | $\delta^{13}\text{C}$ up to ca. +9.4‰ $^{87}\text{Sr}/^{86}\text{Sr}$: 0.7074 | (Misi and Veizer, 1998) |
| Neoproterozoic | Bambuí Group, Brazil | $\delta^{13}\text{C}$ up to ca. +16‰ $^{87}\text{Sr}/^{86}\text{Sr}$: 0.7074 | (Iyer et al., 1995; Misi et al., 2007; Kaufman et al., 2009; Alvarenga et al., 2014; Paula-Santos et al., 2015; Uhlein et al., 2016; Guacaneme et al., 2017; Paula-Santos et al., 2017) |

1991; Derry et al., 1992; Kaufman et al., 1997).

One of the most striking $\delta^{13}\text{C}_{\text{carb}}$ positive excursions is archived in the Neoproterozoic Hüttenberg Formation of northeastern Namibia (i.e., the Hüttenberg anomaly) (Table 1) (Figs. 1–4). Thickly-bedded (> 1000 m) carbonate (mostly dolostone) strata in this formation preserve a remarkable positive excursion in $\delta^{13}\text{C}_{\text{carb}}$ with values up to +12‰ (Kaufman et al., 1991; Kaufman et al., 2009) (Fig. 4). The magnitude of the Hüttenberg anomaly rivals that of a similar $\delta^{13}\text{C}_{\text{carb}}$ positive anomaly (i.e., the Lomagundi Event) associated with the Paleoproterozoic Great Oxidation Event (or GOE) (Schidlowski et al., 1976; Karhu and Holland, 1996; Martin et al., 2013). The biogeochemical drivers for both of these $\delta^{13}\text{C}_{\text{carb}}$ positive anomalies, however, remain highly debated.

Canonical models of the global carbon cycle suggests that $\delta^{13}\text{C}_{\text{carb}}$ positive anomalies likely result from an enhanced rate of organic carbon burial insofar as organic carbon is strongly enriched in ^{12}C (Broecker, 1970; Hayes et al., 1999). Progressive burial of organic matter sequesters ^{12}C in sediments, resulting in both carbonates and subsequent organic matter formed in the oceans to be proportionally enriched in ^{13}C . In the meantime, more organic matter being buried and removed from the Earth surface system also causes a net increase of oxygen in the atmosphere (Broecker, 1970; Derry et al., 1992; Des Marais et al., 1992; Summons and Hayes, 1992; Kump and Arthur, 1999; Ripperdan, 2001). Following this model, the rising limb of the Hüttenberg anomaly may result from enhanced organic carbon burial, and consequently represent a significant oxygenation event; while the falling limb reflects a recovery to pre-anomaly conditions. Notably, a similar model has been applied to the Paleoproterozoic Lomagundi Event (Karhu and Holland, 1996; Planavsky et al., 2012).

Alternatively, the Hüttenberg anomaly can also result from the mixing of high- $\delta^{13}\text{C}_{\text{carb}}$ authigenic carbonates during early diagenesis. This is possible if residual carbon after fermentation (methanogenesis) led to the formation of authigenic carbonates (Claypool and Kaplan, 1974; Irwin et al., 1977; Talbot and Kelts, 1986; Meister et al., 2007; Wehrmann et al., 2011; Birgel et al., 2015; Pierre et al., 2016). Such a process may be more prevalent in the Precambrian ocean where the seawater was mostly anoxic and therefore may promote authigenic carbonate precipitation on the seafloor (Higgins et al., 2009; Schrag et al., 2013).

To test these two hypotheses, we conducted a high resolution chemostratigraphic investigation of a core through the carbonate-dominated succession drilled near to the famed Tsumeb mine in northeastern Namibia. This study reports new chemostratigraphic $\delta^{13}\text{C}_{\text{carb}}$, $\delta^{18}\text{O}_{\text{carb}}$, $\delta^{13}\text{C}_{\text{org}}$, and $\delta^{34}\text{S}_{\text{pyrite}}$ profiles that reveal dramatic stratigraphic

fluctuations. The $\delta^{13}\text{C}_{\text{org}}$ data broadly covary with that of $\delta^{13}\text{C}_{\text{carb}}$ values while the $\delta^{34}\text{S}_{\text{pyrite}}$ profile shows an inverse relationship. We propose that the Hüttenberg anomaly records a local enhancement of global signals. It reflects changes in the primary depositional environment with higher proportional burial of organic carbon, resulting in the buildup of oxygen in the atmosphere, enhanced sulfide oxidation, and an increase in the marine sulfate reservoir.

2. Geological background

The Hüttenberg Formation lies at the top of the Neoproterozoic Otavi Group in northeastern Namibia (Kaufman et al., 2009) (Figs. 1–3). In this region, the thick (> 1000 m) dolostone-dominated succession is well preserved and is archived in a vast library of cores drilled in search of mineralized zones around Tsumeb Mine. The Hüttenberg dolostones around Tsumeb are para-conformably to disconformably overlain by basal shale, siltstone, greywacke, and phyllite with locally interbedded conglomerate beneath the Tschudi Formation of the Mulden Group (Frets, 1969). In northwestern Namibia, however, the Hüttenberg Formation, which overlies the Ghaub (glacial diamictite), Maieberg (cap carbonate), and Elandshoek formations, is generally undifferentiated and largely truncated by siliciclastic molasse associated with the syn-tectonic Mulden Group (Hoffman, 2011).

Based on the stratigraphic relationship between the Ghaub Formation (widely known as a Marinoan glacial diamictite interval) and the position of the Hüttenberg Formation that is located stratigraphically higher, the latter has been regarded to be an Ediacaran interval (Kennedy et al., 1998; Halverson et al., 2005; Hoffman, 2011; Miller, 2013; Prave et al., 2016; Bechstädt et al., 2018). For more details of the overall geology around the studied area, the readers are suggested to refer to the well-published studies (Frets, 1969; Kaufman et al., 1991; Germs, 1995; Hoffmann and Prave, 1996; Hoffman et al., 1998a; Hoffman et al., 2007; Kaufman et al., 2009; Hoffman, 2011; Miller, 2013; Hoffman et al., 2017; Nascimento et al., 2017; Hoffman and Halverson, 2018; Nascimento et al., 2018).

3. Materials and methods

Samples in this study were collected from the S86A drill core from the Tsumeb Mine region in the Otavi Mountainland, northeastern Namibia (Figs. 1–3). The GPS coordinates of this drilled core are 19°14'51.89"S, 17°43'42.17"E. This drill core intersects the entire Hüttenberg Formation reaching a total thickness of ca. 1000 m. Part of the $\delta^{13}\text{C}_{\text{carb}}$ data was previously published for this drill core (Kaufman

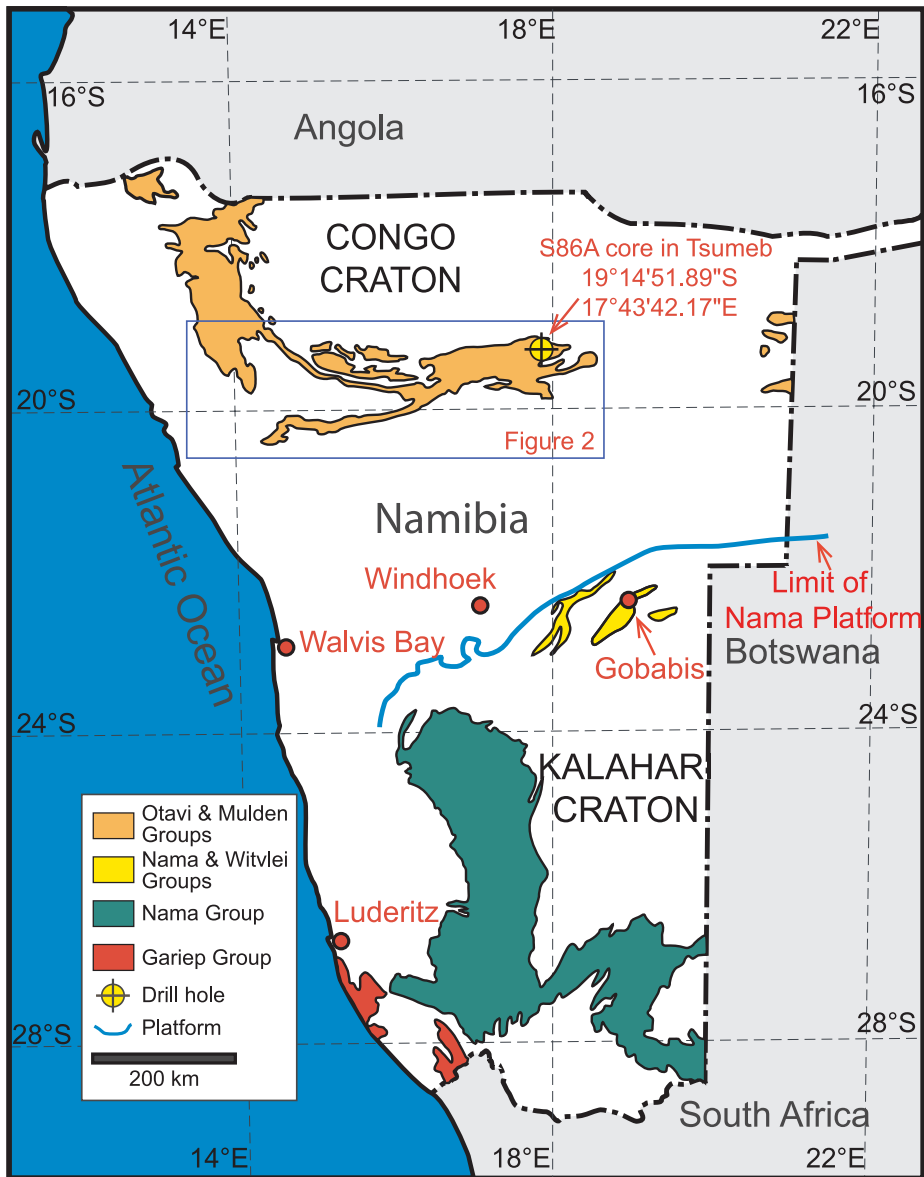


Fig. 1. Geological map of Namibia in southwestern Africa. Samples in this study were collected from the S86A drill core in the Tsumeb Mine region of the Otavi Mountainland, northeastern Namibia. The GPS coordinates of this drilled core are 19°14'51.89"S, 17°43'42.17"E. Modified from Kaufman et al. (1991) and Gorjan et al. (2003). More detailed geological information of the marked rectangle area can be found in Fig. 2.

et al., 2009). In this more comprehensive study, we report new paired carbon and oxygen isotope data ($\delta^{13}\text{C}_{\text{carb}}$, $\delta^{18}\text{O}_{\text{carb}}$), organic carbon (TOC and $\delta^{13}\text{C}_{\text{org}}$) and pyrite sulfur (TS and $\delta^{34}\text{S}_{\text{TS}}$) data, Sr isotope ratios of limestone samples ($^{87}\text{Sr}/^{86}\text{Sr}$), and major and trace elemental abundances (Figs. 5–10).

3.1. $\delta^{13}\text{C}_{\text{carb}}$ and $\delta^{18}\text{O}_{\text{carb}}$ analysis

Carbonate carbon isotope data produced by a continuous flow technique (which did not yield complementary oxygen isotope data) have previously been reported from this drill core (Kaufman et al., 2009). In this study, we further analyzed both carbonate carbon ($\delta^{13}\text{C}_{\text{carb}}$) and oxygen ($\delta^{18}\text{O}_{\text{carb}}$) isotopes from the same batch of drill core samples. Powders for $\delta^{13}\text{C}_{\text{carb}}$ and $\delta^{18}\text{O}_{\text{carb}}$ analyses were collected on polished slabs using a press micro-drill. Micro-drilling was guided by petrographic fabrics so that the finest-grained textures and best preserved zones were sampled. For carbonate $\delta^{13}\text{C}_{\text{carb}}$ and $\delta^{18}\text{O}_{\text{carb}}$ analysis, only fine-grain-sized carbonates were micro-drilled for further geochemical measurement. We indeed found a few horizons with

heavily recrystallized carbonate or quartz veins, but those were strictly avoided during sampling. Both carbon and oxygen isotopes were measured by Gas Bench coupled with Delta plus XP isotope ratio mass spectrometry in the Department of Geological Sciences, Indiana University. The precision for carbon and oxygen isotopes based on repeated measurement of reference materials was routinely better than 0.1‰.

3.2. $\delta^{13}\text{C}_{\text{org}}$ and $\delta^{34}\text{S}_{\text{pyrite}}$ analyses

The organic carbon ($\delta^{13}\text{C}_{\text{org}}$) and pyrite sulfur ($\delta^{34}\text{S}_{\text{pyrite}}$) isotope compositions of bulk powders were measured by combustion of decalcified residues to CO_2 or SO_2 with a Eurovector elemental analyzer inline with an Elementar Isoprime isotope ratio mass spectrometer in the Paleoclimate Laboratory at the University of Maryland. Approximately 15 g of core chips lacking secondary veins or weathered surfaces were crushed and repeatedly (2× or more) acidified with 3 M HCl overnight to quantitatively remove carbonate. These residues were then washed with ultra-pure Milli-Q water to neutral pH, decanted, and dried in an 80 °C oven overnight for subsequent $\delta^{13}\text{C}_{\text{org}}$ and $\delta^{34}\text{S}_{\text{pyrite}}$ analyses.

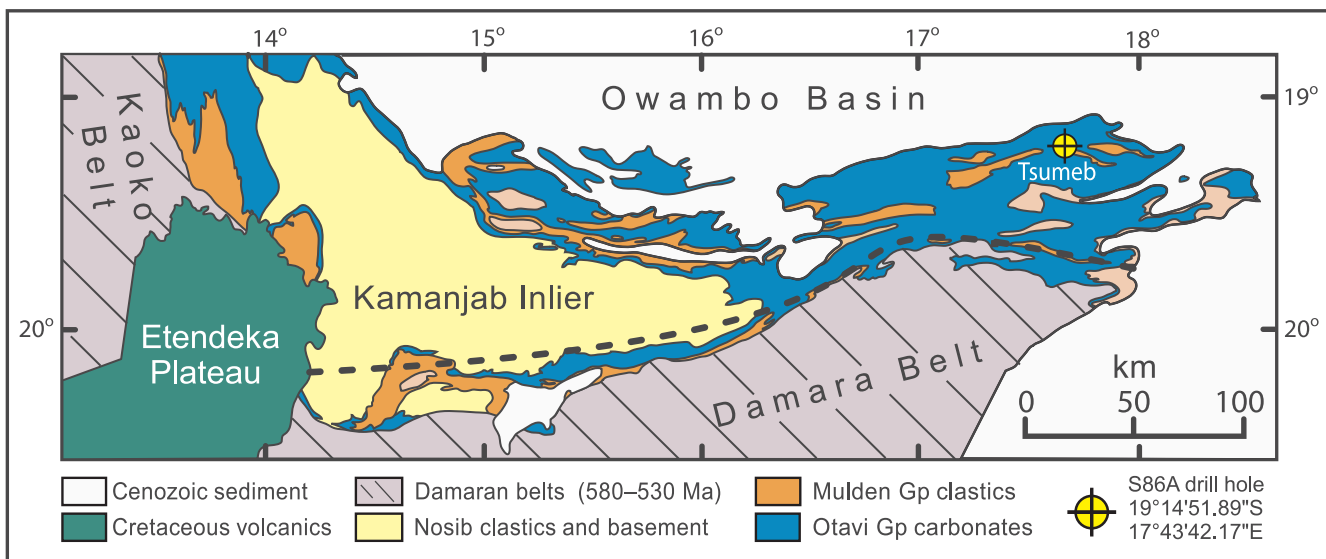


Fig. 2. Detailed geological map of the marked rectangle area in Fig. 1, including the southern arm of the Otavi fold belt, the Kaoko and Damara orogenic belts (Ediacaran to Early Cambrian), the Kamanjab basement inlier (Palaeoproterozoic), the Etendeka volcanic plateau (Early Cretaceous), and the Owambo basin (Cenozoic). The heavy dashed line indicates the platform-foreslope break. Modified from Hoffman (2011).

Given the notable level of ^{13}C enrichment in the Hüttenberg organic matter, we re-acidified a selection of the sample residues with hot, concentrated HCl acid (12 M) to confirm that all carbonates had been consumed, and then decanted, washed, and dried as above. No statistical difference in the ^{13}C abundance of organic matter was found between the two treatments. Total sulfur in the acidified residues was dominated by pyrite, although there may have also been trace amounts of organic sulfur. Uncertainties for $\delta^{13}\text{C}_{\text{org}}$ and $\delta^{34}\text{S}_{\text{pyrite}}$ measurements determined by multiple analyses of standard materials were better than 0.1‰ and 0.3‰, respectively.

3.3. $^{87}\text{Sr}/^{86}\text{Sr}$ analysis

For analysis of strontium isotopic ($^{87}\text{Sr}/^{86}\text{Sr}$) composition, only limestone and dolomitic limestone samples were selected for extraction and measurement. Micro-drilled powders (ca. 5–10 mg) were leached three times in 0.2 M ammonium acetate (pH ~8.2) to remove exchangeable Sr from non-carbonate minerals, and then rinsed three times with Milli-Q water. The leached powder was centrifuged, decanted, and acidified with doubly distilled 0.5 M acetic acid overnight to remove strontium from the carbonate crystal lattice. The supernatant was centrifuged to remove insoluble residues and then decanted, dried, and subsequently dissolved in 200 µl of 3 M HNO₃. Strontium separation by cation exchange was carried out using a small polyethylene column containing ~1 cm thickness of Eichrom®Sr specific resin. Approximately 200–300 ng of the dried sample was transferred onto a degassed and pre-baked (~4.2 A under high vacuum) high purity Re filament with 0.7 µl of Ta₂O₅ activator. The prepared filaments were measured using the VG Sector 54 thermal ionization mass spectrometer in the TIMS facility of the University of Maryland Geochemistry Laboratories. Final data have been corrected for fractionation using the standard value $^{86}\text{Sr}/^{88}\text{Sr} = 0.1194$. No corrections for Rb/Sr ratios have been carried out given the very low Rb/Sr ratios in all the analyzed samples. Repeated analysis of the NBS SRM987 standard yields an average value of $^{87}\text{Sr}/^{86}\text{Sr} = 0.710245 \pm 0.000011$ (2σ) during the analytical window.

3.4. Elemental concentration analysis

Major and trace elemental abundances of micro-drilled carbonates were analyzed for a few representative samples in order to better

evaluate the degree of diagenetic alteration. Aliquots of the micro-drilled carbonate powders were dissolved in 0.4 M HNO₃, centrifuged, and only analyzed for the solutions. Any clays, if present, would not have been dissolved by the dilute acid. The resulting solutions were analyzed on a Thermo Scientific® iCAP-Q ICP-MS (Inductively Coupled Plasma – Mass Spectrometry) at the Carnegie Institution of Washington. Precision of these analyses as determined by repeated measurements of a house standard carbonate was < 5% (2σ) for major elements with high concentrations and < 10% (2σ) for trace elements and REEs.

4. Geochemical results

All the new data in this study are shown in Figs. 5–10, and can be found in the [Online Supplementary Material](#).

4.1. $\delta^{13}\text{C}_{\text{carb}}$ and $\delta^{18}\text{O}_{\text{carb}}$ data

The studied drill core is dominated by almost pure dolostones with carbonate percentages (wt%) approaching 100% (Fig. 5A). The $\delta^{13}\text{C}_{\text{carb}}$ profile reveals a remarkable positive excursion beginning around +2‰ in the Elandshoek Formation and rising up to +12‰ in the Hüttenberg Formation before recovering back to ca. 0‰ near the Hüttenberg/Tschudi boundary (Fig. 5C). The $\delta^{13}\text{C}_{\text{carb}}$ values remain high, but fluctuate rapidly between +6 and +12‰ in the middle of the succession. In contrast, the $\delta^{18}\text{O}_{\text{carb}}$ profile (reveals relatively less variation, ranging from -8 to -2‰, with three notable cycles through the succession (Fig. 5B).

4.2. $\delta^{13}\text{C}_{\text{org}}$, $\Delta^{13}\text{C}_{\text{carb-org}}$ and TOC data

Although more variable, the $\delta^{13}\text{C}_{\text{org}}$ profile shows a general parallel trend with the paired $\delta^{13}\text{C}_{\text{carb}}$ values (Fig. 6B). The calculated carbon isotope fractionations ($\Delta^{13}\text{C}_{\text{carb-org}}$) show fluctuations between 20‰ and 30‰ (Fig. 6D). The TOC values are generally low most likely due to carbonate dilution, but we note that organic abundances broadly track the $\delta^{13}\text{C}_{\text{carb}}$ trend in the Hüttenberg Formation (Fig. 6E).

4.3. $\delta^{34}\text{S}_{\text{pyrite}}$ and TS data

The $\delta^{34}\text{S}_{\text{pyrite}}$ profile shows a broadly antithetic trend with that of $\delta^{13}\text{C}_{\text{carb}}$ compositions (Fig. 7C). Highly positive $\delta^{34}\text{S}_{\text{pyrite}}$ values (up to



Fig. 3. Google map view of the studied S86A drill core. The GPS coordinates of this drilled core are 19°14'51.89"S, 17°43'42.17"E.

+30‰) at both the base and the top of the succession are associated with the onset and decline of the Hüttenberg anomaly, while significant $\delta^{34}\text{S}$ depletion in pyrite ($\delta^{34}\text{S}_{\text{pyrite}}$ down to -10‰) is associated with the sustained positive $\delta^{13}\text{C}_{\text{carb}}$ plateau. The TS (Fig. 7D) abundances in these core samples are generally low, which is most likely a function of carbonate dilution. Nonetheless, there is an overall positive excursion in TS with the highest abundances associated with peak $\delta^{13}\text{C}_{\text{carb}}$ values.

4.4. Cross-plots of C, O and S isotope and concentration data

Cross-plots of the different C and S isotope or concentration values were also conducted in order to explore the relationship between different data set (Fig. 8). The cross-plots of $\delta^{13}\text{C}_{\text{carb}}$ vs. $\delta^{13}\text{C}_{\text{org}}$ ($R^2 = 0.33$), $\delta^{13}\text{C}_{\text{carb}}$ vs. $\delta^{34}\text{S}_{\text{pyrite}}$ ($R^2 = 0.21$), and $\delta^{13}\text{C}_{\text{org}}$ vs. $\Delta^{13}\text{C}$ ($R^2 = 0.40$) show visible correlations (Fig. 8A–C), while the cross-plots of $\delta^{13}\text{C}_{\text{carb}}$ vs. $\delta^{18}\text{O}_{\text{carb}}$, $\delta^{13}\text{C}_{\text{org}}$ vs. TOC, $\delta^{34}\text{S}_{\text{pyrite}}$ vs. TS, TOC vs. TS, $\delta^{34}\text{S}_{\text{pyrite}}$ vs. $\delta^{13}\text{C}_{\text{org}}$, and $\delta^{34}\text{S}_{\text{pyrite}}$ vs. TOC do not show clear correlations (Fig. 8D–I).

4.4.1. $^{87}\text{Sr}/^{86}\text{Sr}$ and elemental concentration data

Although the ~1000-m-thick drill core is dominated by dolostones, 15 samples of limestones or dolomitic limestones were identified by

testing with 5% HCl acid. In this study, only limestone and dolomitic limestones samples were analyzed for $^{87}\text{Sr}/^{86}\text{Sr}$, major (Ca, Mg) and trace elemental (e.g., Fe, Mn, Rb, Sr, Al and REEs) compositions (Figs. 9, 10). The lowest $^{87}\text{Sr}/^{86}\text{Sr}$ value determined for the sample set was 0.7074.

Major and trace elemental concentrations were also analyzed in order to evaluate the diagenetic effect on the $^{87}\text{Sr}/^{86}\text{Sr}$ data (Figs. 9, 10). The cross-plots of $^{87}\text{Sr}/^{86}\text{Sr}$ vs. Rb/Sr ($R^2 = 0.53$), $^{87}\text{Sr}/^{86}\text{Sr}$ vs. Mn/Sr ($R^2 = 0.44$), $^{87}\text{Sr}/^{86}\text{Sr}$ vs. Fe/Sr ($R^2 = 0.44$), $^{87}\text{Sr}/^{86}\text{Sr}$ vs. Al/Sr ($R^2 = 0.47$), $^{87}\text{Sr}/^{86}\text{Sr}$ vs. Mg/Ca ($R^2 = 0.75$), and Mg/Ca vs. Rb/Sr ($R^2 = 0.46$) all show clear positive correlations (Fig. 10A–F). The cross-plot of Ca vs. Mg concentrations shows a negative correlation (Fig. 10G). The measured $^{87}\text{Sr}/^{86}\text{Sr}$ data do not show clear correlation with corresponding $\delta^{13}\text{C}_{\text{carb}}$ or $\delta^{18}\text{O}_{\text{carb}}$ data (Fig. 10H–I).

5. Discussion

5.1. Diagenetic evaluation

5.1.1. Evaluating $\delta^{13}\text{C}_{\text{carb}}$ and $\delta^{18}\text{O}_{\text{carb}}$ data

Typically, $\delta^{18}\text{O}_{\text{carb}}$ values could be more easily altered than $\delta^{13}\text{C}_{\text{carb}}$ compositions due to different alteration thresholds during

Comparison of the Hüttenberg $\delta^{13}\text{C}_{\text{carb}}$ positive anomaly at different sections in Namibia

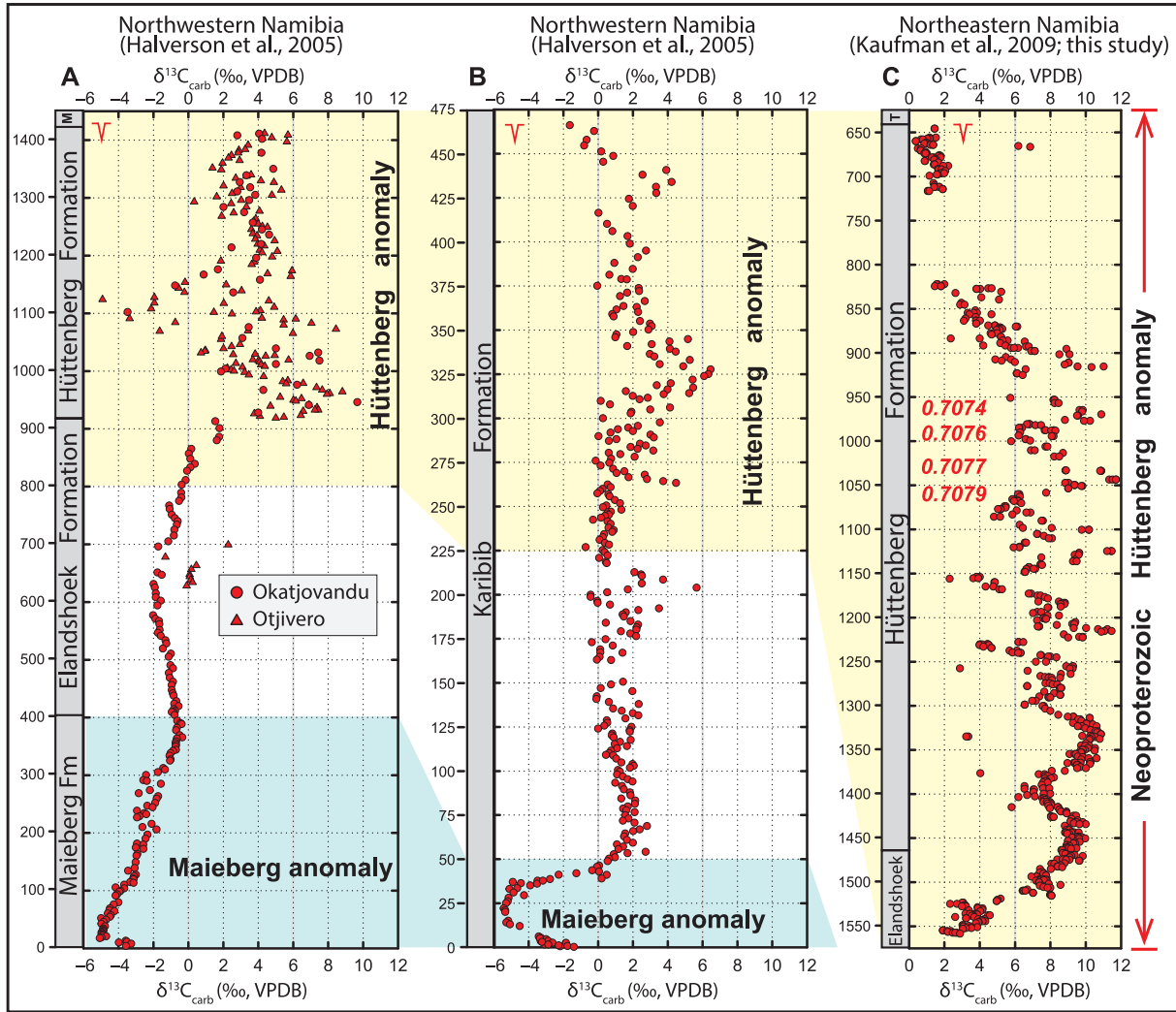


Fig. 4. Comparisons of the $\delta^{13}\text{C}_{\text{carb}}$ profiles of the Hüttenberg anomaly in Namibia. Data in panels A and B are from Halverson et al. (2005); Data in panel C are from Kaufman et al. (2009) and this study. M = Mulden Group; T = Tschudi Formation.

fluid-water interaction (Jacobsen and Kaufman, 1999). However, the chemostratigraphic $\delta^{18}\text{O}_{\text{carb}}$ profile of the studied Hüttenberg drill core shows largely consistent values of between $-8\text{\textperthousand}$ and $-2\text{\textperthousand}$ (Fig. 5B), which speaks to limited diagenetic effect on the $\delta^{13}\text{C}_{\text{carb}}$ and $\delta^{18}\text{O}_{\text{carb}}$ values.

The cross-plot of $\delta^{13}\text{C}_{\text{carb}}$ vs. $\delta^{18}\text{O}_{\text{carb}}$ has been widely used as a tool to evaluate the influence of diagenetic process, especially meteoric water diagenesis and organic-matter-associated post-depositional diagenesis in carbonate samples (e.g., Talbot and Kelts, 1986; Gischler et al., 2007; Knauth and Kennedy, 2009; Derry, 2010; Bishop et al., 2014; Cui et al., 2017). Typically, a positive correlation in $\delta^{13}\text{C}_{\text{carb}}$ vs. $\delta^{18}\text{O}_{\text{carb}}$ cross-plot can be produced by progressive alteration by ^{18}O -depleted meteoric water and ^{13}C -depleted late porewater due to organic matter re-oxidation. However, the $\delta^{13}\text{C}_{\text{carb}}$ vs. $\delta^{18}\text{O}_{\text{carb}}$ cross-plot of the Hüttenberg carbonates does not show correlation (Fig. 8G), which suggests little impact by diagenesis. Thus, we tentatively exclude the possibility that the chemostratigraphic fluctuations in the $\delta^{13}\text{C}_{\text{carb}}$ and $\delta^{18}\text{O}_{\text{carb}}$ profiles (Fig. 5) were caused by post-depositional processes.

5.1.2. Evaluating $\delta^{13}\text{C}_{\text{org}}$ data

Compared with the published Ediacaran $\delta^{13}\text{C}_{\text{org}}$ data (e.g., Fike et al., 2006; McFadden et al., 2008; Ader et al., 2009; Lee et al., 2013; Cui et al., 2015; Cui et al., 2016a; Cui et al., 2016b; Cui et al., 2016c; Cui et al., 2017), the organic matter in the Hüttenberg Formation appears to be more enriched in ^{13}C . The measured high $\delta^{13}\text{C}_{\text{org}}$ values (Fig. 6B) could potentially be caused by mixed carbonates due to an incomplete acidification. However, during the sample preparation for $\delta^{13}\text{C}_{\text{org}}$ analysis, all the samples were acidified by 3 M HCl until no more bubbles were produced after adding extra HCl acid in order to achieve a complete acidification. To further evaluate the quality of our $\delta^{13}\text{C}_{\text{org}}$ data, we also re-analyzed many samples by acidifying the samples with pure HCl acid. The reanalyzed sample show consistent $\delta^{13}\text{C}_{\text{org}}$ data with earlier data. Therefore, we rule out the possibility of incomplete acidification as the cause of high $\delta^{13}\text{C}_{\text{org}}$ values in this study.

5.1.3. Evaluating $^{87}\text{Sr}/^{86}\text{Sr}$ data

For these limestone and dolomitic limestone samples, both $^{87}\text{Sr}/^{86}\text{Sr}$ and trace elemental (e.g., Fe, Mn, Rb, Sr, Al and REEs) compositions

Carbon and oxygen isotope compositions of the Hüttenberg anomaly, northeastern Namibia

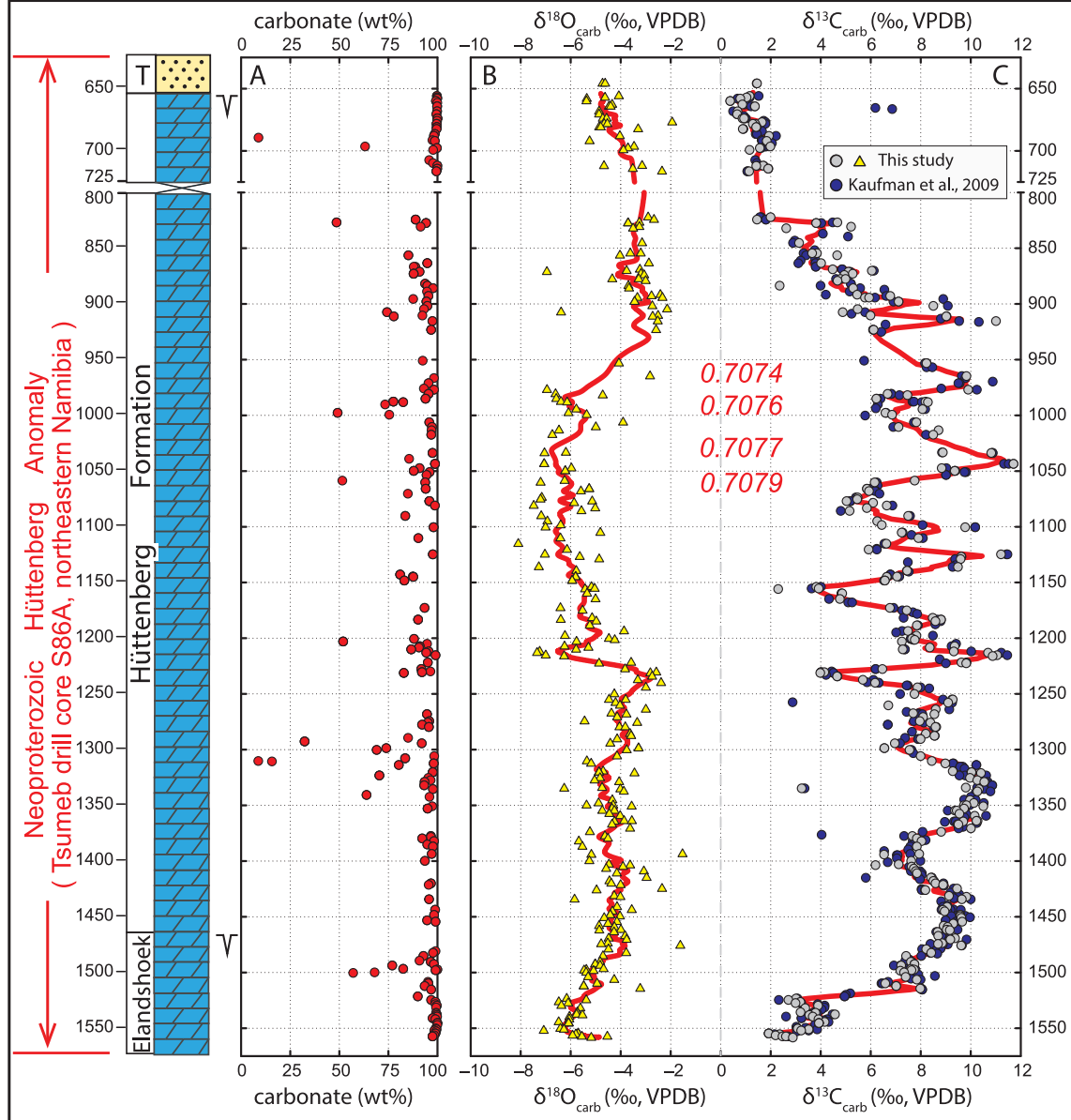


Fig. 5. Chemostratigraphic profiles of the Hüttenberg anomaly. Measured geochemical data include carbonate percentage (wt%), carbonate carbon ($\delta^{13}\text{C}_{\text{carb}}$, ‰ VPDB) and oxygen isotopes ($\delta^{18}\text{O}_{\text{carb}}$, ‰ VPDB). The $\delta^{13}\text{C}_{\text{carb}}$ data in blue circles are from Kaufman et al. (2009); the $\delta^{13}\text{C}_{\text{carb}}$ data in gray circles and their corresponding $\delta^{18}\text{O}_{\text{carb}}$ data are newly analyzed in this study. Fitted lines represent six-point running average. T = Tschudi Formation. All the data can be found in the Online Supplementary Material.

were analyzed. The negative or positive correlations between different elemental ratios and the $^{87}\text{Sr}/^{86}\text{Sr}$ data (Fig. 10A–G) can be explained by different degrees of diagenesis. Generally, $^{87}\text{Sr}/^{86}\text{Sr}$ would progressively increase as more ^{87}Sr derived from ^{87}Rb decay is mixed into the carbonate lattice during burial diagenesis (Kaufman et al., 1993; Banner, 1995). It is possible that the correlations found in our data result from progressive diagenesis (e.g., dolomitization). Therefore, the lowest $^{87}\text{Sr}/^{86}\text{Sr}$ value of 0.7074 is taken as the most accurate record of seawater $^{87}\text{Sr}/^{86}\text{Sr}$ composition during deposition.

In summary, diagenesis affected somewhat the $^{87}\text{Sr}/^{86}\text{Sr}$ values whereas the $\delta^{13}\text{C}_{\text{carb}}$, $\delta^{18}\text{O}_{\text{carb}}$, $\delta^{13}\text{C}_{\text{org}}$, and $\delta^{34}\text{S}_{\text{pyrite}}$ trends were unaffected by diagenesis hence record primary geochemical signals.

5.2. Controlling factors of the $\delta^{13}\text{C}_{\text{carb}}$ values

Controlling factors that may have contributed to high $\delta^{13}\text{C}_{\text{carb}}$ values could be multiple. Increased $\delta^{13}\text{C}$ of carbon input, enhanced carbon isotope fractionations ($\Delta^{13}\text{C}_{\text{carb-org}}$), larger proportion of organic carbon burial, and redox stratifications could all possibly increase the $\delta^{13}\text{C}_{\text{carb}}$ values during deposition (Shields et al., 2002). In addition, local evaporative environmental conditions could also cause high $\delta^{13}\text{C}_{\text{carb}}$ values, which has been reported in both modern environments (Schidlowski et al., 1984; Stiller et al., 1985; Valero-Garcés et al., 1999; Gomez et al., 2014; Guo and Chafetz, 2014; Birgel et al., 2015; Horton et al., 2015) and deep-time records (Klaebe et al., 2016). However, no

Paired carbonate carbon and organic carbon isotope compositions of the Hüttenberg anomaly, Namibia

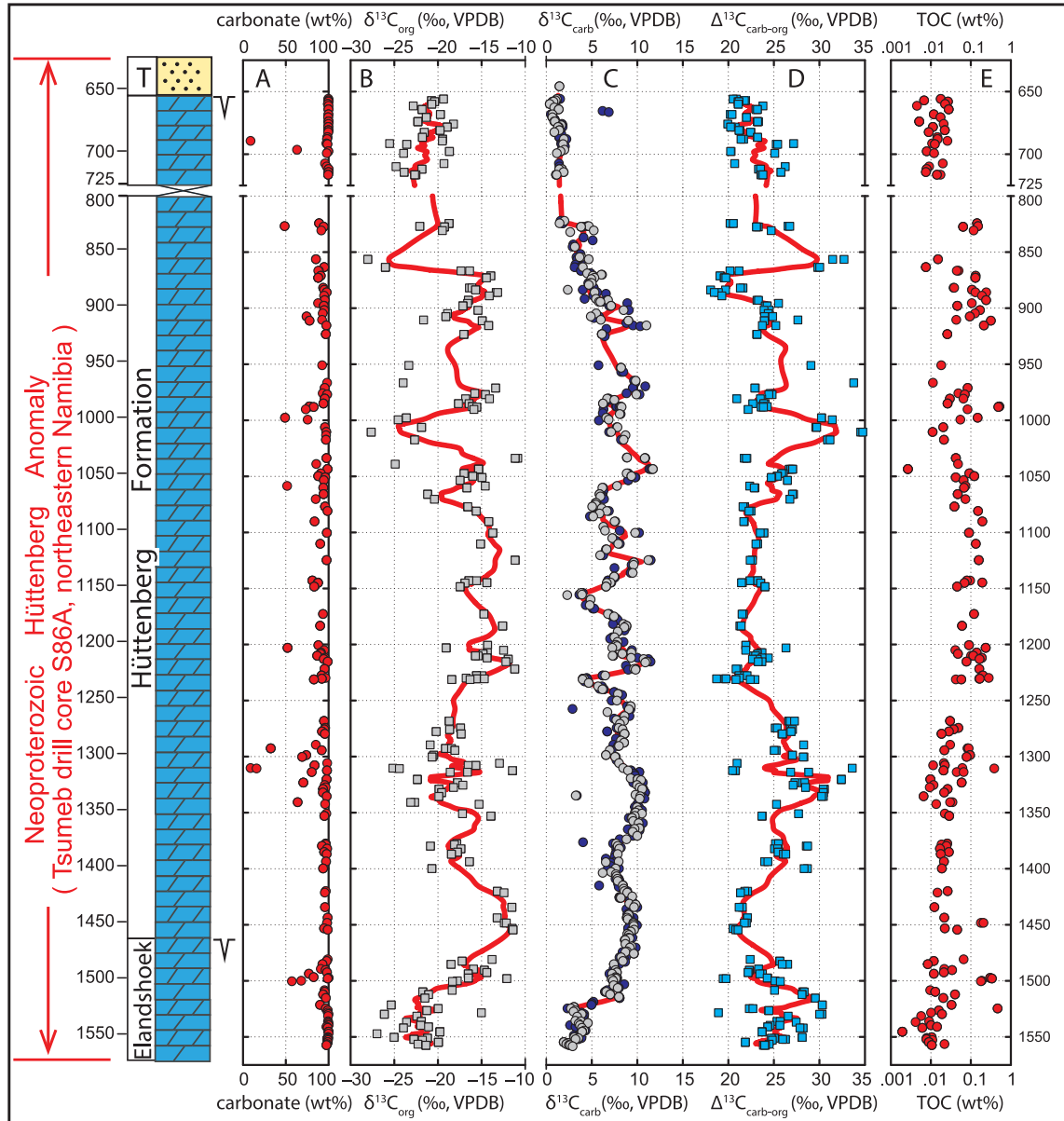


Fig. 6. Chemostratigraphic carbon isotope profiles of the Hüttenberg anomaly. Measured geochemical data include carbonate percentage (carbonate wt%), carbonate carbon ($\delta^{13}\text{C}_{\text{carb}}$, ‰ VPDB), organic carbon isotopes ($\delta^{13}\text{C}_{\text{org}}$, ‰ VPDB), carbon isotope fractionations ($\Delta^{13}\text{C}_{\text{carb-org}}$), total organic carbon content (TOC%). The $\delta^{13}\text{C}_{\text{carb}}$ data in blue circles are from Kaufman et al. (2009); the $\delta^{13}\text{C}_{\text{carb}}$ values in gray circles are new in this study. Fitted lines represent six-point running average. T = Tschudi Formation. All the data can be found in the [Online Supplementary Material](#).

diagnostic evidence for evaporative conditions, for example, pseudomorphs or lenses and beds of evaporites (e.g., Pope and Grotzinger, 2003; Duda et al., 2015; Cui et al., 2016b; Klaebe et al., 2016), were found in the studied drill cores. The dominating lithology in the studied drill core is dolomiticrite. Moreover, evaporation-induced ^{18}O and ^{13}C enrichment often shows a positive correlation in $\delta^{13}\text{C}_{\text{carb}}$ vs. $\delta^{18}\text{O}_{\text{carb}}$ (Talbot, 1990; Li and Ku, 1997; Gomez et al., 2014; Guo and Chafetz, 2014; Horton et al., 2015). Such a correlation is not seen in the studied Hüttenberg carbonates (Fig. 8G). Therefore, it is unlikely that evaporation-induced fractionation in $\delta^{13}\text{C}_{\text{carb}}$ plays a dominant role in causing the Hüttenberg anomaly, but this hypothesis is suggested to be further tested in future studies.

Enhanced carbonate weathering could also possibly cause $\delta^{13}\text{C}_{\text{carb}}$ positive anomalies on platform environments by increasing the $\delta^{13}\text{C}$ of local carbon input (Kump et al., 1999; Melchin and Holmden, 2006; Fan et al., 2009). Additionally, it was more recently proposed that tectonic controls on the long-term carbon isotope mass balance can be potential factors for the ancient carbon cycles (Shields, 2017; Shields and Mills, 2017). During periods of low denudation rates, $\delta^{13}\text{C}$ values tend to be higher (Shields and Mills, 2017). Using a thermal subsidence model for the Otavi Group, the Hüttenberg anomaly is estimated to have lasted over 15 million years (Kaufman et al., 2009). It is possible that long-term factors are involved in the genesis of the Hüttenberg anomaly. Although no evidence for a changing weathering rate was found so far

Anti-correlation of carbon and sulfur isotope compositions during the Hüttenberg anomaly, Namibia

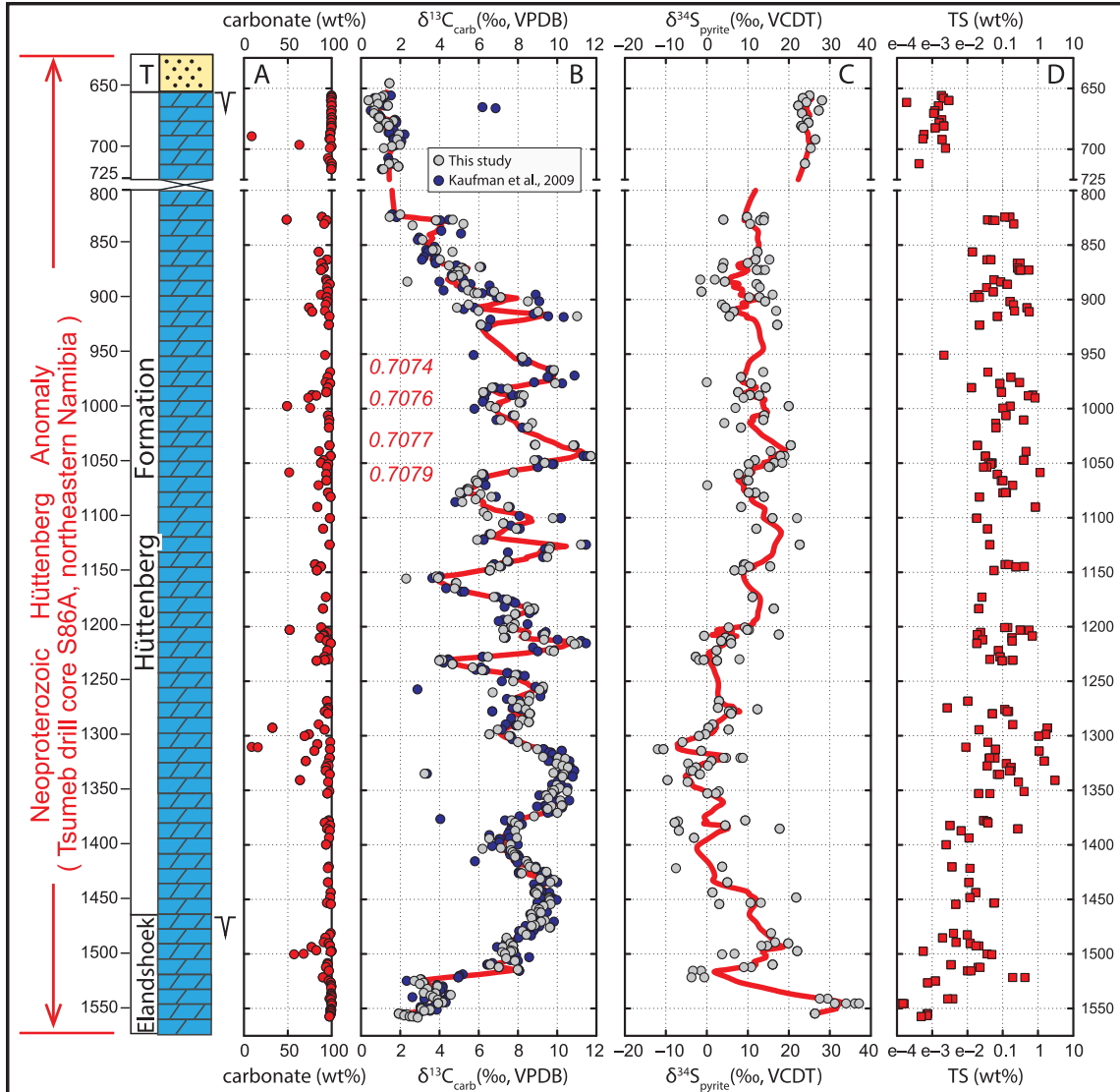


Fig. 7. Chemostratigraphic carbon and sulfur isotope profiles of the Hüttenberg anomaly. Measured geochemical data include carbonate percentage (wt%), carbonate carbon ($\delta^{13}\text{C}_{\text{carb}}$, ‰ VPDB), total sulfur isotopes of acidified residuals ($\delta^{34}\text{S}_{\text{pyrite}}$, ‰ VCDT; including pyrite and trace amount of organic S), total sulfur content (TS%, dominated by pyrite with trace amount of organic S). The $\delta^{13}\text{C}_{\text{carb}}$ values in blue circles are from Kaufman et al. (2009); the $\delta^{13}\text{C}_{\text{carb}}$ values in gray circles are new in this study. Fitted lines represent six-point running average. T = Tschudi Formation. All the data can be found in the [Online Supplementary Material](#).

in the studied Hüttenberg drill cores, we regard it as a testable hypothesis for future studies. Investigations on Ca, Mg isotopes (e.g., Pokrovsky et al., 2011; Kasemann et al., 2014), and Li isotopes (e.g., Misra and Froelich, 2012; von Strandmann et al., 2013; Lechner et al., 2015) may hold the potential to evaluate the weathering conditions during the Hüttenberg anomaly.

5.3. Primary or authigenic signals?

In light of the new data, we propose that the Hüttenberg $\delta^{13}\text{C}_{\text{carb}}$ positive anomaly (Figs. 4, 5) results from a primary perturbation of the marine dissolved inorganic carbon (DIC) reservoir, instead of an authigenic event as suggested by Schrag et al. (2013). The supporting

evidence is listed below.

- (1) The broad co-variation between $\delta^{13}\text{C}_{\text{carb}}$ and $\delta^{13}\text{C}_{\text{org}}$ values (Fig. 6) supports a profound change in seawater where photosynthesis is the main mechanism in fractionating carbon isotopes. Although diagenesis that can change both $\delta^{13}\text{C}_{\text{carb}}$ and $\delta^{13}\text{C}_{\text{org}}$ in the same direction was found in modern marine sediments at the Great Bahama Bank (Oehlert and Swart, 2014), no diagenetic process in the Precambrian is known that can shift both porewater DIC and DOC in the same direction with similar levels of rate and magnitude (Knoll et al., 1986).
- (2) Coupled $\delta^{13}\text{C}_{\text{carb}}$ and $\delta^{34}\text{S}_{\text{pyrite}}$ excursions further support changes in seawater, instead of porewater, signals. Authigenic process in the

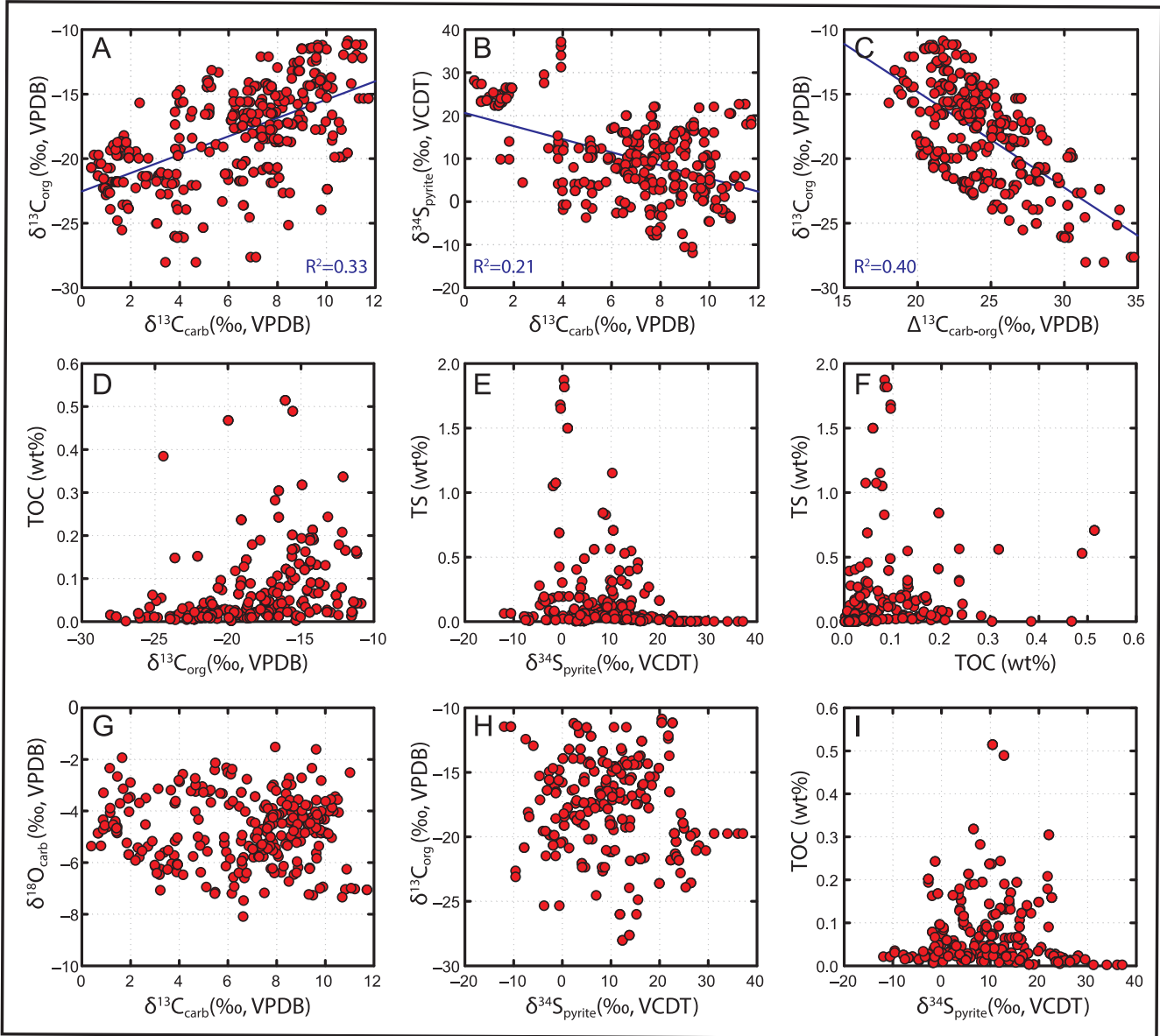


Fig. 8. Cross plots of the data shown in Figs. 5–7. See detailed discussion in the main text. All the data can be found in the [Online Supplementary Material](#).

zone of methanogenesis could drive pore water alkalinity to higher $\delta^{13}\text{C}$ compositions (Irwin et al., 1977; Meister et al., 2007; Birgel et al., 2015). However, in the same porewater environment, the $\delta^{34}\text{S}_{\text{pyrite}}$ signals should also increase due to Rayleigh fractionation associated with progressive microbial sulfate reduction (MSR) (Borowski et al., 2013; Fike et al., 2015). Insofar as we see the opposite trend, the stratigraphically prolonged inverse $\delta^{13}\text{C}$ – $\delta^{34}\text{S}$ relationship (Fig. 7) argues against an authigenic origin for carbonates in the Hüttenberg anomaly.

5.4. Local environmental controls on the Hüttenberg anomaly

Compared with many other Ediacaran successions, the Hüttenberg anomaly shows distinct features in chemostratigraphy. First, the $\delta^{13}\text{C}_{\text{carb}}$ profile of the Hüttenberg anomaly does not fit into the well-established Ediacaran $\delta^{13}\text{C}_{\text{carb}}$ record at a global scale. The $\delta^{13}\text{C}_{\text{carb}}$

plateau of +12‰ in the Hüttenberg anomaly stands out relative to other Ediacaran successions. It is notable that the Hüttenberg $\delta^{13}\text{C}_{\text{carb}}$ anomaly is missing in the well-studied Ediacaran Doushantuo and Dengying formations in China (Jiang et al., 2007; Zhou and Xiao, 2007; Zhu et al., 2007; McFadden et al., 2008; Wang et al., 2012; Lu et al., 2013; Zhu et al., 2013; Cui et al., 2015; Cui et al., 2016a; Cui et al., 2016b; Wang et al., 2016; Cui et al., 2017) and many other Ediacaran sections elsewhere (Kaufman et al., 1991; Kaufman and Knoll, 1995; Knoll et al., 1995; Saylor et al., 1998; Walter et al., 2000; Fike et al., 2006; Narbonne et al., 2012; Macdonald et al., 2013; Wood et al., 2015; Bold et al., 2016; Cui et al., 2016a; Xiao et al., 2016; Zhu et al., 2017).

Second, it has been predicted that the Ediacaran Hüttenberg Formation should have $^{87}\text{Sr}/^{86}\text{Sr}$ signals at around 0.7085 (Kennedy et al., 1998). However, new $^{87}\text{Sr}/^{86}\text{Sr}$ analysis in this study shows values as low as 0.7074 in limestone samples of the Hüttenberg drill cores (Fig. 9). The $^{87}\text{Sr}/^{86}\text{Sr}$ value of 0.7074 is in strong contrast

Geochemical analyses of thin limestone and dolomitic limestone layers in the dolostone-dominated Hüttenberg Formation, northeastern Namibia

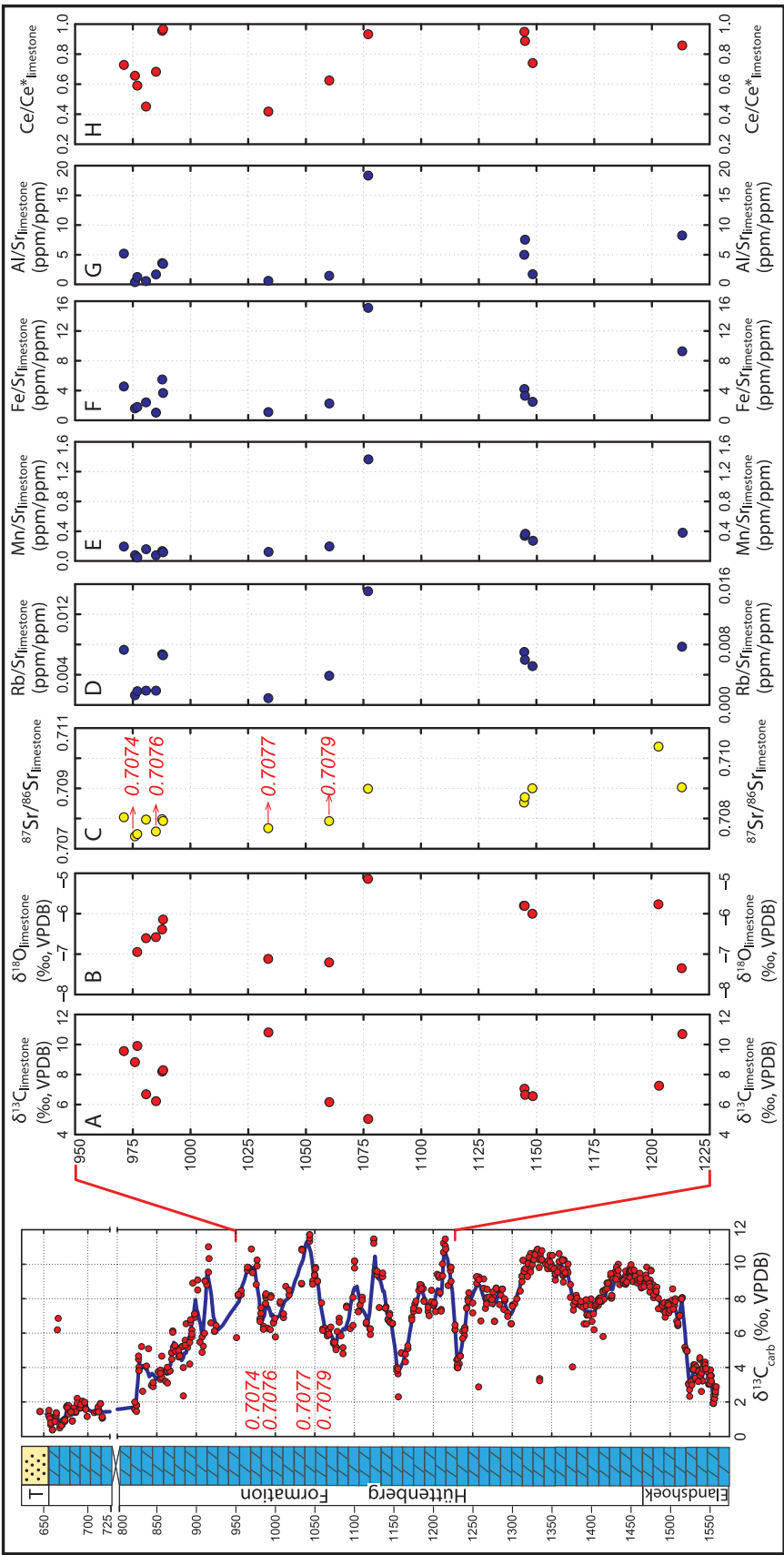


Fig. 9. Chemostratigraphic $^{87}\text{Sr}/^{86}\text{Sr}$ and trace element profiles of the studied S86A drill cores. Although the studied drill cores are dominated by dolostones, 15 layers of limestone or dolomitic limestone samples were found and analyzed for $^{87}\text{Sr}/^{86}\text{Sr}$ and trace element concentrations in this study. Ce anomaly (Ce/Ce^*) values were calculated using the formula $\text{Ce}/\text{Ce}^* = \text{Ce}_{\text{PAAAS}}/(\text{Pr})_{\text{PAAAS}}^2/[\text{Nd}]_{\text{PAAAS}}$ (Ling et al., 2013). All the data can be found in the [Online Supplementary Material](#).

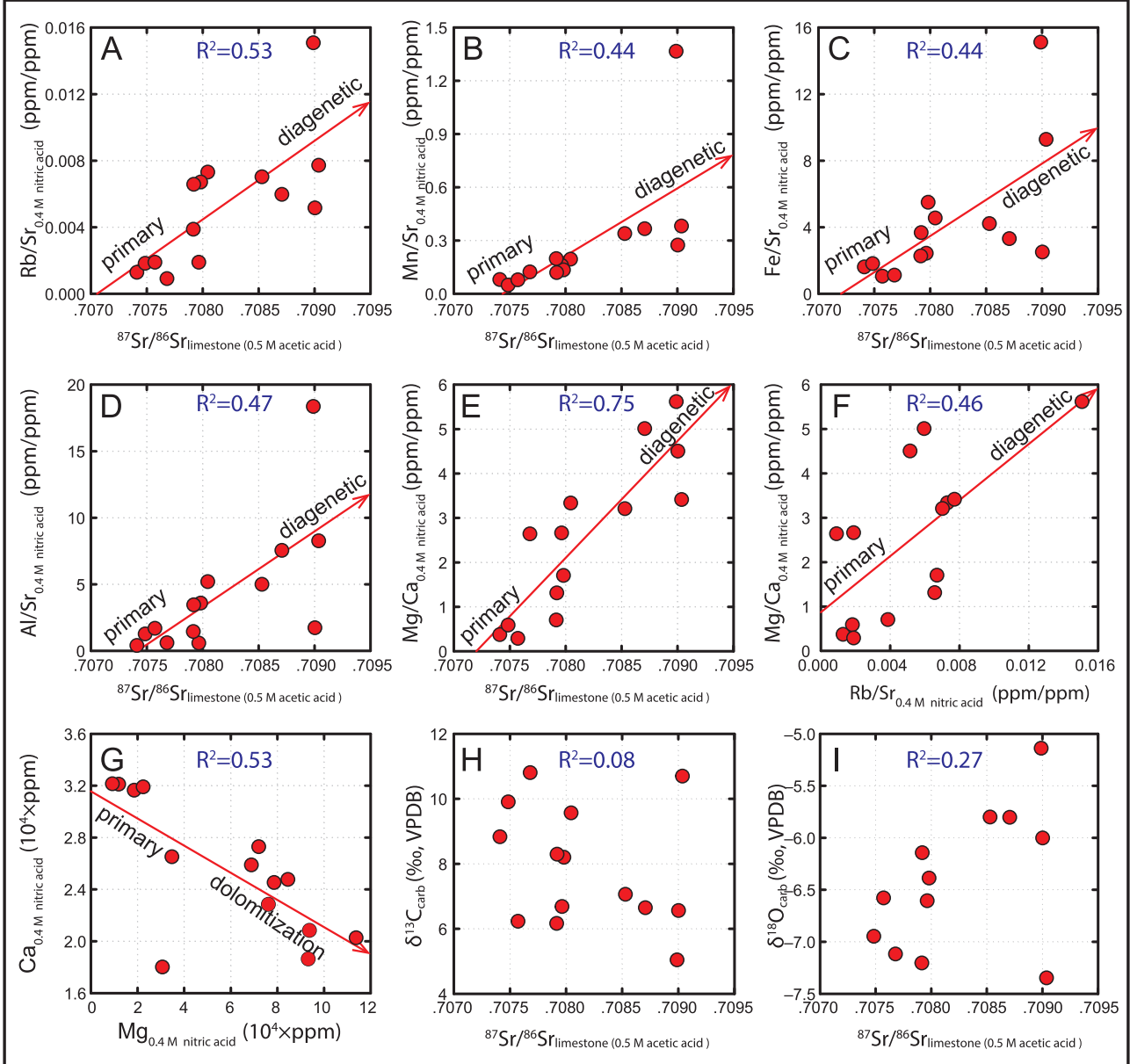


Fig. 10. Cross plots of the isotope and elemental concentration data measured from limestone or dolomitic limestone samples within the Hüttenberg Formation. See detailed discussion in the main text. All the data can be found in the [Online Supplementary Material](#).

with the typical Ediacaran seawater $^{87}\text{Sr}/^{86}\text{Sr}$ values that range between 0.7080 and 0.7090 (Burns et al., 1994; Narbonne et al., 1994; Kaufman et al., 1997; Calver, 2000; Jiang et al., 2007; Melezhik et al., 2009; Sawaki et al., 2010; Cui et al., 2015; Cui et al., 2016a; Xiao et al., 2016; Cui et al., 2017). Therefore, it appears that both the $\delta^{13}\text{C}_{\text{carb}}$ and the $^{87}\text{Sr}/^{86}\text{Sr}$ signals in the studied Hüttenberg drill cores are deviated significantly from the typical Ediacaran profile.

The most parsimonious interpretation of these distinct features is that the Hüttenberg Formation does not record open ocean signals of the Ediacaran Period. It is possible that the Hüttenberg anomaly formed in a restricted basin with $\delta^{13}\text{C}_{\text{carb}}$ and $^{87}\text{Sr}/^{86}\text{Sr}$ signals that are significantly deviated from the global Ediacaran

ocean (Fig. 11). Conditions with enhanced evaporation and a high influx of sulfate into the basin due to pyrite oxidation may have caused the $\delta^{13}\text{C}_{\text{carb}}$ positive excursion and the $\delta^{34}\text{S}_{\text{pyrite}}$ negative excursion, respectively.

5.5. Inverse $\delta^{13}\text{C}$ - $\delta^{34}\text{S}$ pattern in response to an oxygenation event

New data in this study show a notable anti-correlation in the $\delta^{13}\text{C}$ and $\delta^{34}\text{S}$ profiles (Fig. 7). The inverse $\delta^{13}\text{C}$ - $\delta^{34}\text{S}$ relationship in marine C-S cycling is common in Phanerozoic successions, but is rare in Precambrian time (Hayes et al., 1992). Theoretically, ocean redox conditions should either promote or inhibit the burial of reduced phases (i.e., organic carbon and pyrite sulfur) collectively, thereby driving the

Biogeochemical model 1: Local environmental controls on the Hüttenberg anomaly

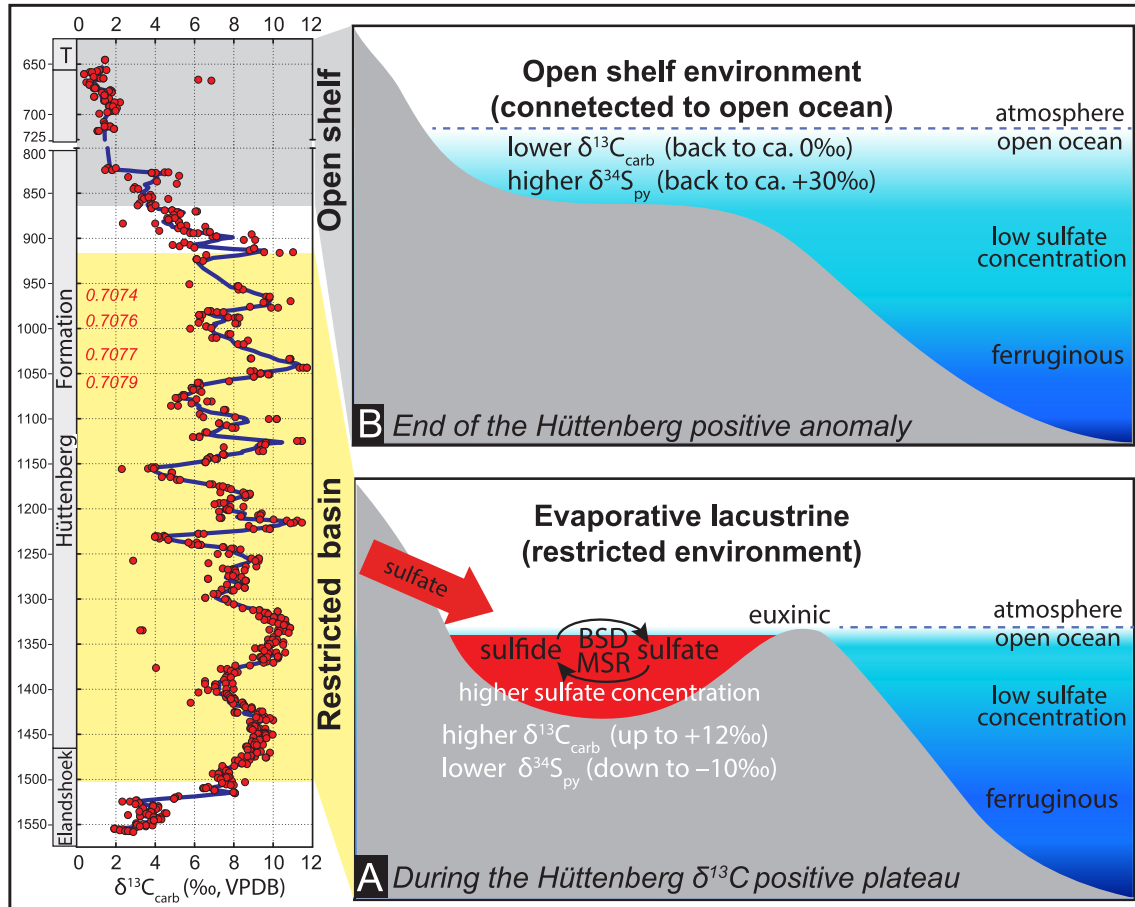


Fig. 11. Biogeochemical model for the local environmental controls of the Hüttenberg anomaly during (A) the $\delta^{13}\text{C}_{\text{carb}}$ plateau and (B) the end of the Hüttenberg anomaly. Model in A is characterized by a restricted basin environment with an enhanced evaporation and a higher influx of sulfate. Model in B is characterized by an open ocean environment.

coupled directional changes of seawater $\delta^{13}\text{C}$ and $\delta^{34}\text{S}$ compositions (e.g., Gill et al., 2011; Jones and Fike, 2013).

The inverse relationship has been referred to as the “central dilemma of C–S geochemistry” (Holser et al., 1988). Mass balance modeling suggests that the inverse $\delta^{13}\text{C}$ – $\delta^{34}\text{S}$ pattern in Phanerozoic sediments is driven by a coupling in the burial of reduced carbon and oxidized sulfur (e.g., gypsum) (Berner, 1989). For the Precambrian, this mechanism is difficult to evaluate given the dearth of marine evaporite deposits. Nonetheless, marine sulfate abundances may have swung dramatically associated with oceanic redox changes during the Precambrian (Planavsky et al., 2012; Blättler et al., 2018; Ossa Ossa et al., 2018). For example, the inverse $\delta^{13}\text{C}$ – $\delta^{34}\text{S}$ pattern preserved during the Lomagundi Event may be associated with fluctuations of the oceanic sulfate reservoir (Planavsky et al., 2012; Ossa Ossa et al., 2018). An earlier study on the Neoproterozoic evaporites shows an overall negative correlation between the $\delta^{34}\text{S}_{\text{sulfate}}$ and $\delta^{13}\text{C}_{\text{carb}}$ curves, which may indicate the operation of an exogenic sulfur cycle (Strauss, 1993).

We propose that the inverse stratigraphic $\delta^{13}\text{C}_{\text{carb}}$ – $\delta^{34}\text{S}_{\text{pyrite}}$ relationship of the Hüttenberg anomaly (Fig. 7) may reflect oxygenation–deoxygenation of surface environments and the buildup–contraction of oceanic sulfate reservoirs (Fig. 12). As a byproduct of photosynthesis, the rise of oxygen is consistent with the paired carbon isotope excursions in carbonates and co-existing organic matter.

Considering that enhanced sulfate concentration could promote S isotope fractionations (Habicht et al., 2002; Crowe et al., 2014), the antithetic negative excursion in $\delta^{34}\text{S}_{\text{pyrite}}$ likely results from the rise of oceanic sulfate, an expected consequence of enhanced oxidative weathering of terrestrial pyrite (e.g., Kaufman et al., 2007). Sulfate concentrations may also be enhanced in the upper water column by bacterial sulfur disproportionation (BSD) in a stratified ocean (Canfield and Teske, 1996), which may have also contributed to the decrease of the Hüttenberg $\delta^{34}\text{S}_{\text{pyrite}}$ values (Fig. 12A).

Supporting evidence for this interpretation also comes from the organic carbon and total sulfur abundances in the studies drill core. Although the overall TOC and TS values are very low (Fig. 6E, 7D), which is likely due to significant dilution by carbonates in this dolostone-dominated strata, the relatively higher TOC and TS abundances in the $\delta^{13}\text{C}_{\text{carb}}$ plateau (Fig. 6E, 7D) further suggest that the Hüttenberg anomaly may be associated with the expansion of oceanic anoxia (and potentially euxinia) during deposition (Fig. 12A).

In summary, we propose that the stratigraphic isotope trends can be interpreted as a record of enhanced organic matter burial and pyrite re-oxidation during an atmospheric oxygenation event (Fig. 12A). Conversely, the falling limb of the positive $\delta^{13}\text{C}_{\text{carb}}$ excursion reflects the drawdown of oxygen and marine sulfate reservoir during the end of the Hüttenberg anomaly (Fig. 12B).

Biogeochemical model 2: Global environmental controls on the Hüttenberg anomaly

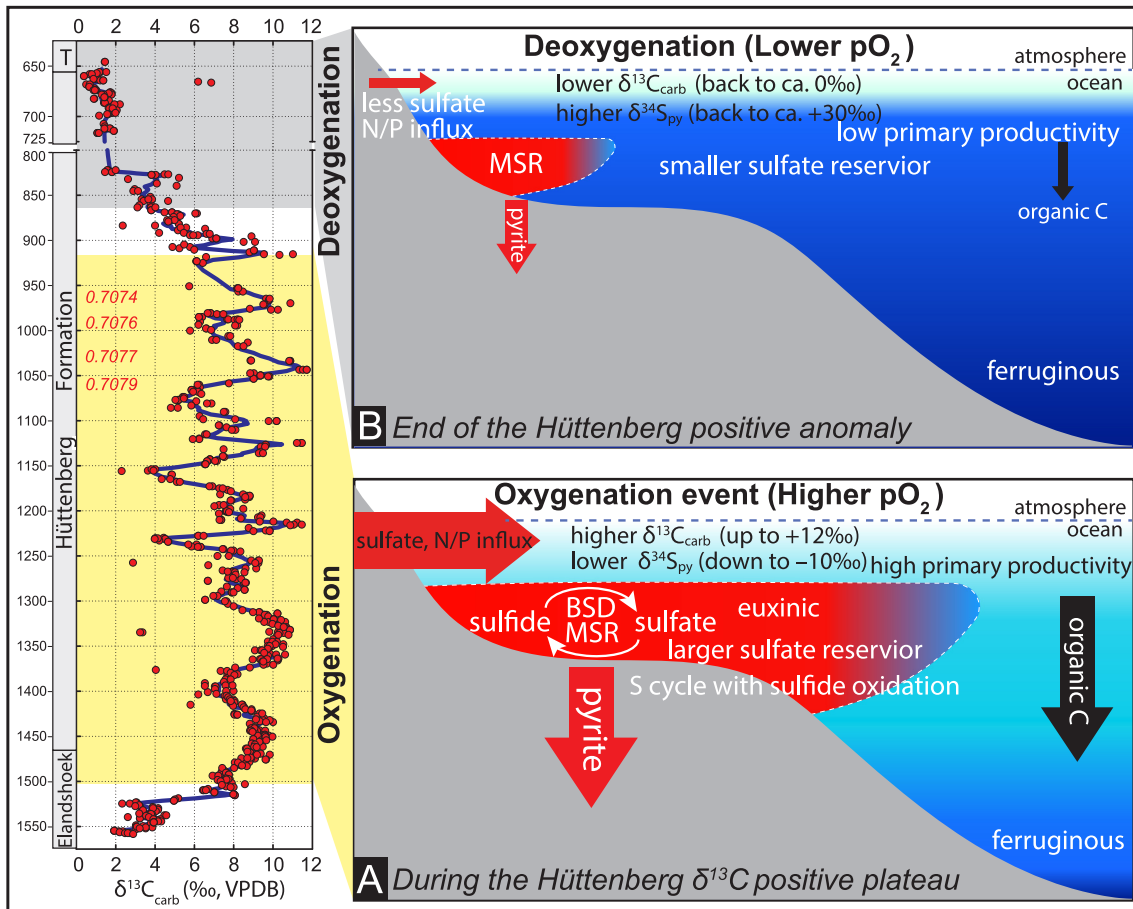


Fig. 12. Biogeochemical model for the global environmental controls of the Hüttenberg anomaly during (A) the $\delta^{13}\text{C}_{\text{carb}}$ plateau and (B) the end of the Hüttenberg anomaly. Model in A is characterized by an oxygenation event with high burial rate of organic carbon and enhanced oxidative weathering of pyrite. Model in B is characterized by a deoxygenation event with a drawdown of marine sulfate reservoir and a recovery to pre-anomaly conditions.

5.6. A stepwise pattern of the Neoproterozoic oxygenation event

Considering that both local and global environmental controls may have played a role in causing the observed isotope signatures (Figs. 11, 12), we propose that the Hüttenberg anomaly records a local enhancement of global oxygenation signals. The local and global environmental factors considered in this study are not mutually exclusive. This interpretation is consistent with multiple studies of the Ediacaran strata elsewhere that also suggest oxygenation events in the Ediacaran ocean (Sahoo et al., 2012; Sahoo, 2015; Sahoo et al., 2016; Zhou et al., 2016).

In this study, we also compared the Hüttenberg anomaly with other Neoproterozoic strata at a global scale. The strata we considered include the Tayshir Formation in Mongolia (Fig. 13) (Brasier et al., 1996a; Brasier et al., 1996b; Macdonald et al., 2009; Bold et al., 2016), the Keele Formation in Canada (Fig. 14) (Eisbacher, 1985; Aitken, 1991a; Aitken, 1991b; Narbonne and Aitken, 1995; James et al., 2001; Day et al., 2004), and the Etina Formation in Australia (Fig. 15) (Gorjan et al., 2000; Walter et al., 2000; McKirdy et al., 2001; Swanson-Hysell et al., 2010; Rose et al., 2012; Verdel and Campbell, 2017), all of which have been widely regarded as Cryogenian (pre-Marinoan) strata.

Regardless of the age difference between the Ediacaran Hüttenberg anomaly and the Cryogenian $\delta^{13}\text{C}_{\text{carb}}$ positive anomalies, the

similarities in chemostratigraphy indicate similar biogeochemical conditions and a stepwise pattern of the Neoproterozoic Oxygenation Event. Notably, both the Tayshir $\delta^{13}\text{C}_{\text{carb}}$ positive anomaly (Fig. 13) and the Keele anomaly (Fig. 14) record sustained high $\delta^{13}\text{C}_{\text{carb}}$ values of around +10‰ and similar $^{87}\text{Sr}/^{86}\text{Sr}$ values of around 0.7074 (Narbonne et al., 1994; Brasier et al., 1996a; Brasier et al., 1996b; Kaufman et al., 1997; Shields et al., 1997; Shields et al., 2002; Macdonald et al., 2009; Bold et al., 2016). Moreover, the Etina anomaly is also characterized by sustained high $\delta^{13}\text{C}_{\text{carb}}$ values of ca. +10‰, an overall $\delta^{34}\text{S}_{\text{pyrite}}$ negative excursion down to ca. -10‰, and similar $^{87}\text{Sr}/^{86}\text{Sr}$ values (Fig. 15) (Gorjan et al., 2000; Walter et al., 2000; McKirdy et al., 2001; Swanson-Hysell et al., 2010; Rose et al., 2012), though the stratigraphic resolution of the Etina $\delta^{34}\text{S}_{\text{pyrite}}$ profile is relatively low compared with the Hüttenberg $\delta^{34}\text{S}_{\text{pyrite}}$ profile in this study (Fig. 7).

Taken together, it is possible that the Ediacaran Hüttenberg anomaly in Namibia reflects similar biogeochemical conditions with the Cryogenian $\delta^{13}\text{C}_{\text{carb}}$ positive anomalies. The pulsed occurrence of these $\delta^{13}\text{C}_{\text{carb}}$ positive anomalies during the Neoproterozoic suggests a stepwise pattern of the Neoproterozoic Oxygenation Event. These oxygenation events may have facilitated the emergence of early life at that time (Yuan et al., 2011; Yuan et al., 2013; Guan et al., 2014; Wan et al., 2016; Anderson et al., 2017).

Carbonate carbon isotope and $^{87}\text{Sr}/^{86}\text{Sr}$ profiles of the Cryogenian Tayshir positive anomaly in Mongolia

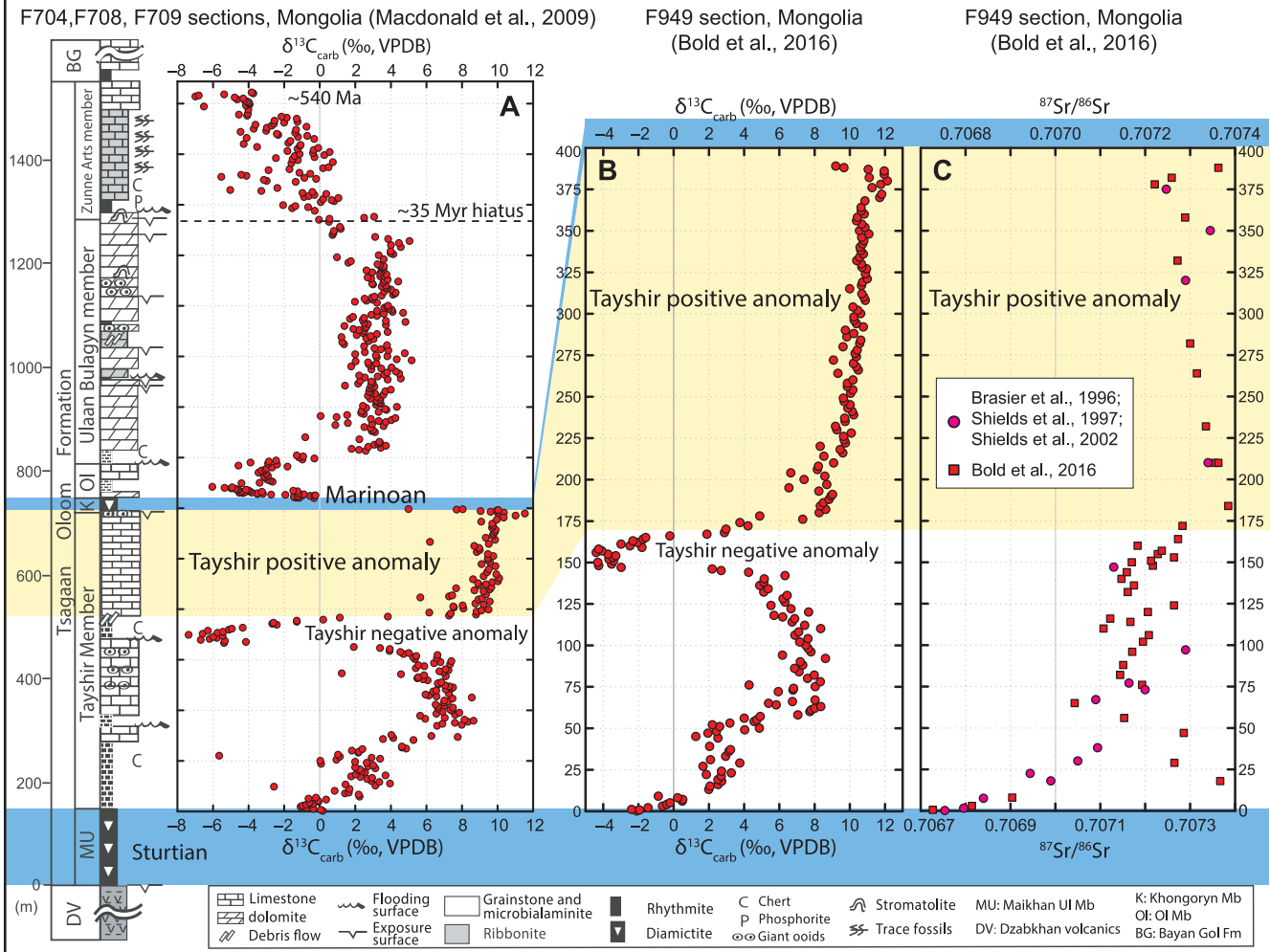


Fig. 13. Chemostratigraphic profiles of the pre-Marinoan Tayshir $\delta^{13}\text{C}_{\text{carb}}$ positive anomaly (highlighted yellow interval). Regardless of different ages, both the Ediacaran Hüttenberg anomaly and the Cryogenian Tayshir $\delta^{13}\text{C}_{\text{carb}}$ positive anomaly are characterized by sustained high $\delta^{13}\text{C}_{\text{carb}}$ values of around +10‰ and $^{87}\text{Sr}/^{86}\text{Sr}$ values of around 0.7074, indicating similar biogeochemical conditions. Data source: lithology column and data in A (Macdonald et al., 2009); Data in B (Bold et al., 2016); Data in C (Brasier et al., 1996; Shields et al., 1997; Shields et al., 2002; Bold et al., 2016).

6. Conclusions

The Neoproterozoic Hüttenberg anomaly in northeastern Namibia shows remarkable perturbations in C and S isotopes. Our new data in this study reveal that the $\delta^{13}\text{C}_{\text{carb}}$ positive excursion is coupled with a broad $\delta^{13}\text{C}_{\text{org}}$ positive excursion and a large $\delta^{34}\text{S}_{\text{pyrite}}$ negative excursion (Figs. 5–7). These isotopic coupling suggests a primary perturbation of the marine dissolved inorganic carbon (DIC) reservoir during deposition, instead of an authigenic event occurring in porewater environments.

Both local and global environmental factors may have contributed to the Hüttenberg anomaly (Figs. 11, 12). On one hand, the Hüttenberg anomaly may reflect restricted basin signals that are deviated from the Ediacaran open ocean; on the other hand, the Ediacaran Hüttenberg anomaly, together with the Cryogenian $\delta^{13}\text{C}_{\text{carb}}$ positive excursions (Figs. 13–15), suggests a stepwise pattern of the Neoproterozoic Oxygenation Event. The Hüttenberg anomaly may therefore record a local enhancement of global oxygenation signals. Our data support the emerging view that the Neoproterozoic Oxygenation Event of the Earth

surface environment may have facilitated the evolution of early life at that time.

Acknowledgements

This research is supported by funding from the Sigma Xi Grants-in-Aid Program to HC, the NASA Exobiology Program (NNX12AR91G) to AJK, the NSF Sedimentary Geology and Paleontology program (EAR0844270 and EAR1528553) to AJK. We thank Arno Günzel, Kirsten Günzel, Jeanita Potgieter, Erenst Tjitta, and Les Kriesfeld for access, sampling, and photography of the S86A core in 1999 and 2016; Richard Walker and Igor Puchtel for the guidance of Sr isotope measurements in the UMD Isotope Geochemistry Laboratory; Paul Hoffman, Tony Prave, Francis Macdonald, Galen Halverson, Graham Shields-Zhou, Thilo Bechstädt, and Chuanming Zhou for helpful discussion and comments. This paper benefits from constructive reviews by three anonymous reviewers. We also thank Randall Parrish (editor) and Susannah Porter (associate editor) for handling this manuscript.

Paired carbon isotopes and $^{87}\text{Sr}/^{86}\text{Sr}$ profiles of the Cryogenian Keele positive anomaly, NW Canada

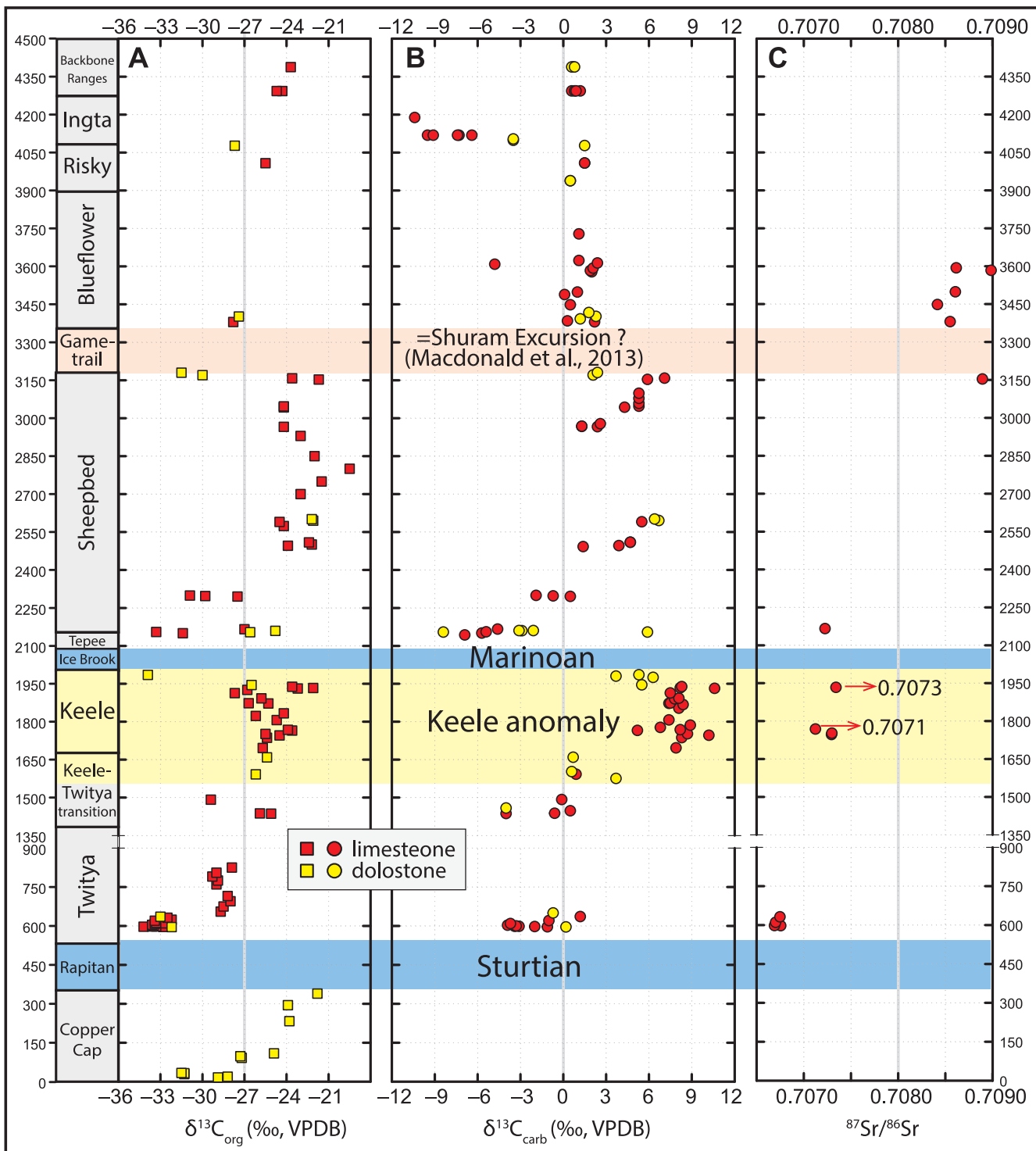


Fig. 14. Chemostratigraphic profiles of the pre-Marinoan Keele anomaly (highlighted yellow interval). Regardless of different ages, both the Ediacaran Hüttenberg anomaly and the Cryogenian Keele anomaly are characterized by sustained $\delta^{13}\text{C}_{\text{carb}}$ positive values of ca. +10‰ and similar $^{87}\text{Sr}/^{86}\text{Sr}$ values, indicating similar biogeochemical conditions. The Gametrail Formation has been proposed to be correlative with the Ediacaran Shuram Excursion (Macdonald et al., 2013). Data Source: (Narbonne et al., 1994; Kaufman et al., 1997).

Carbonate carbon and pyrite sulfur isotope profiles of the Cryogenian Etina $\delta^{13}\text{C}$ positive anomaly in Australia

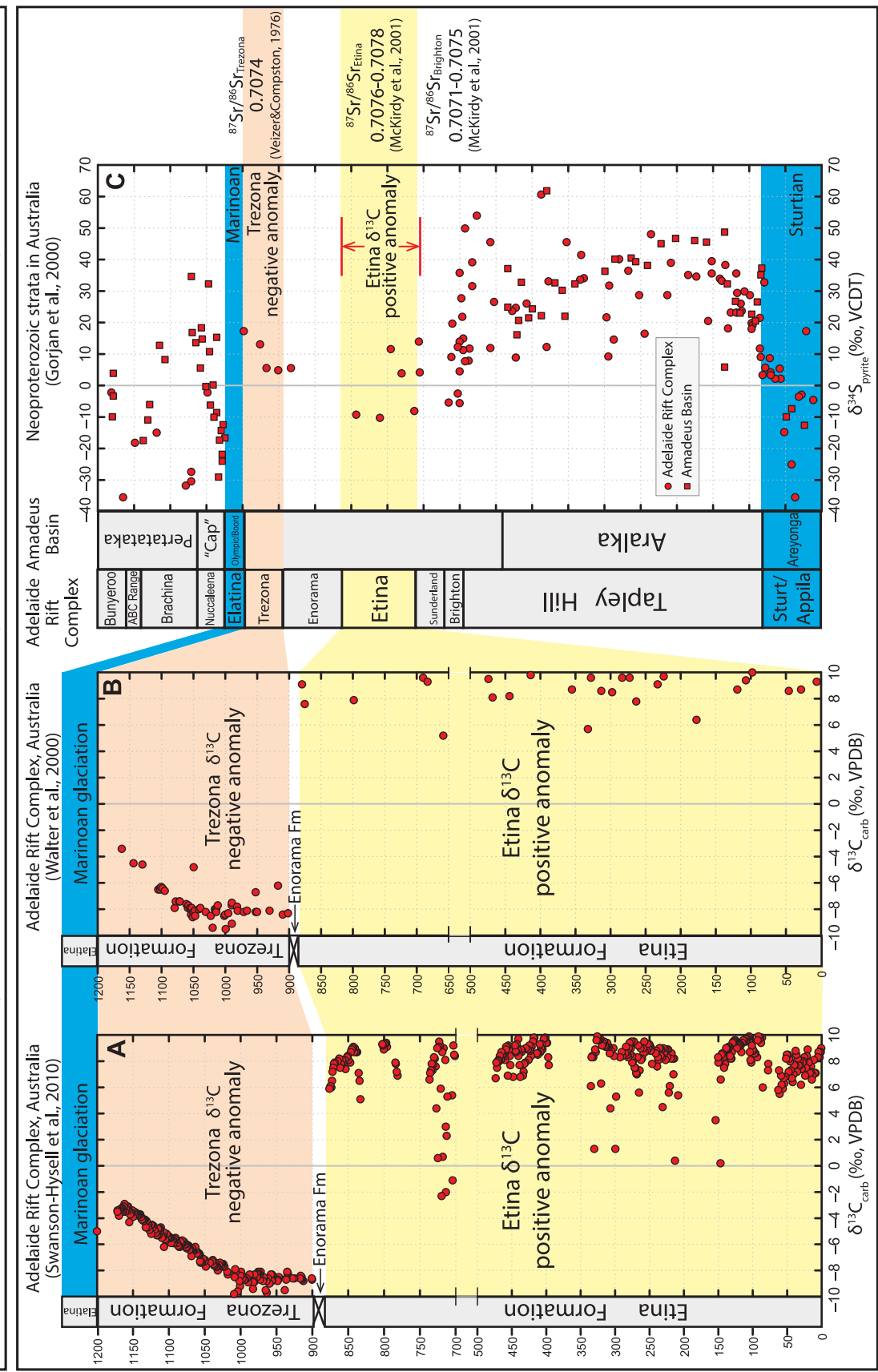


Fig. 15. Chemostratigraphic profiles of the pre-Marinoan Etina anomaly (highlighted yellow interval). Regardless of different ages, both the Ediacaran Hüttenberg anomaly and the Cryogenian Etina anomaly are characterized by sustained high $\delta^{13}\text{C}_{\text{carb}}$ values of ca. +10‰, and similar $\delta^{34}\text{S}_{\text{pyrite}}$ negative excursion down to ca. -10‰, and similar ${}^{87}\text{Sr}/{}^{86}\text{Sr}$ values, indicating similar biogeochemical conditions. Data source: Data in A (Swanson-Hysell et al., 2010); Data in B (Walter et al., 2000); $\delta^{34}\text{S}_{\text{pyrite}}$ data in C (Gorjan et al., 2000); ${}^{87}\text{Sr}/{}^{86}\text{Sr}$ data (Veizer and Compston, 1976; McKinley et al., 2001).

Appendix A. Supplementary data

Supplementary data associated with this article can be found, in the online version, at <http://dx.doi.org/10.1016/j.precamres.2018.05.024>.

References

- Ader, M., Macouin, M., Trindade, R.I.F., Hadrien, M.-H., Yang, Z., Sun, Z., Besse, J., 2009. A multilayered water column in the Ediacaran Yangtze platform? Insights from carbonate and organic matter paired $\delta^{13}\text{C}$. *Earth Planet. Sci. Lett.* 288, 213–227. <http://dx.doi.org/10.1016/j.epsl.2009.09.024>.
- Atikten, J.D., 1991a. Two late Proterozoic glaciations, Mackenzie Mountains, north-western Canada. *Geology* 19, 445–448. [http://dx.doi.org/10.1130/0091-7613\(1991\)019<0445:tptgmm>2.3.co;2](http://dx.doi.org/10.1130/0091-7613(1991)019<0445:tptgmm>2.3.co;2).
- Atikten, J.D., 1991b. The Ice Brook Formation and Post-Rapitan, Late Proterozoic glaciation, Mackenzie Mountains, Northwest Territories. *Geol. Surv. Canada Bull.* 404 404, 43 Ottawa, Canada.
- Alvarenga, C.J.S., Santos, R.V., Vieira, L.C., Lima, B.A.F., Mancini, L.H., 2014. Mesoproterozoic isotope stratigraphy on carbonates platforms in the Brasilia Belt of Brazil. *Precambr. Res.* 251, 164–180. <http://dx.doi.org/10.1016/j.precamres.2014.06.011>.
- Anderson, R.P., McMahon, S., Bold, U., Macdonald, F.A., Briggs, D.E., 2017. Palaeobiology of the early Ediacaran Shuurgat Formation, Zavkhan Terrane, south-western Mongolia. *J. Syst. Paleontol.* 15, 947–968. <http://dx.doi.org/10.1080/14772019.2016.1259272>.
- Banner, J.L., 1995. Application of the trace element and isotope geochemistry of strontium to studies of carbonate diagenesis. *Sedimentology* 42, 805–824. <http://dx.doi.org/10.1111/j.1365-3091.1995.tb00410.x>.
- Bechstädt, T., Jäger, H., Rittersbacher, A., Schweisfurth, B., Spence, G., Werner, G., Boni, M., 2018. The Cryogenian Ghaub Formation of Namibia – new insights into Neoproterozoic glaciations. *Earth Sci. Rev.* 177, 678–714. <http://dx.doi.org/10.1016/j.earscirev.2017.11.028>.
- Berner, R.A., 1989. Biogeochemical cycles of carbon and sulfur and their effect on atmospheric oxygen over phanerozoic time. *Palaeogeogr. Palaeoclimatol. Palaeoecol.* 75, 97–122. [http://dx.doi.org/10.1016/0031-0182\(89\)90186-7](http://dx.doi.org/10.1016/0031-0182(89)90186-7).
- Birgel, D., Meister, P., Lundberg, R., Horath, T.D., Bontognali, T.R.R., Bahniuk, A.M., de Rezende, C.E., Vasconcelos, C., McKenzie, J.A., 2015. Methanogenesis produces strong $\delta^{13}\text{C}$ enrichment in stromatolites of Lagoa Salgada, Brazil: a modern analogue for Palaeo-/Neoproterozoic stromatolites? *Geobiology* 13, 245–266. <http://dx.doi.org/10.1111/gbi.12130>.
- Bishop, J.W., Osleger, D.A., Montañez, I.P., Sumner, D.Y., 2014. Meteoric diagenesis and fluid-rock interaction in the Middle Permian Capitan backreef: Yates Formation, Slaughter Canyon, New Mexico. *AAPG Bull.* 98, 1495–1519. <http://dx.doi.org/10.1306/05201311158>.
- Blättler, C.L., Claire, M.W., Prave, A.R., Kirsimäe, K., Higgins, J.A., Medvedev, P.V., Romashkin, A.E., Rychanchik, D.V., Zerkle, A.L., Paiste, K., Kreitsmann, T., Millar, I.L., Hayles, J.A., Bao, H., Turchyn, A.V., Warke, M.R., Lepland, A., 2018. Two-billion-year-old evaporites capture Earth's great oxidation. *Science* 360, 320–323. <http://dx.doi.org/10.1126/science.aar2687>.
- Bold, U., Smith, E.F., Rooney, A.D., Bowring, S.A., Buchwaldt, R., Dudás, F.Ó., Ramezani, J., Crowley, J.L., Schrag, D.P., Macdonald, F.A., 2016. Neoproterozoic stratigraphy of the Zavkhan terrane of Mongolia: the backbone for Cryogenian and early Ediacaran chemostratigraphic records. *Am. J. Sci.* 316, 1–63. <http://dx.doi.org/10.2475/01.2016.01>.
- Borowski, W.S., Rodriguez, N.M., Paull, C.K., Ussler III, W., 2013. Are $\delta^{34}\text{S}$ -enriched authigenic sulfide minerals a proxy for elevated methane flux and gas hydrates in the geologic record? *Mar. Pet. Geol.* 43, 381–395. <http://dx.doi.org/10.1016/j.marpetgeo.2012.12.009>.
- Brasier, M.D., Dorjnamjaa, D., Lindsay, J., 1996a. The Neoproterozoic to early Cambrian in southwest Mongolia: an introduction. *Geol. Mag.* 133, 365–369. <http://dx.doi.org/10.1017/s0016756800007548>.
- Brasier, M.D., Shields, G., Kuleshov, V.N., Zhegallo, E.A., 1996b. Integrated chemo- and biostratigraphic calibration of early animal evolution: Neoproterozoic-early Cambrian of southwest Mongolia. *Geol. Mag.* 133, 445–485. <http://dx.doi.org/10.1017/s0016756800007603>.
- Broecker, W.S., 1970. A boundary condition on the evolution of atmospheric oxygen. *J. Geophys. Res.* 75, 3553–3557. <http://dx.doi.org/10.1029/JC075i018p03553>.
- Burns, S.J., Haudenschild, U., Matter, A., 1994. The strontium isotopic composition of carbonates from the late Precambrian (~560–540 Ma) Huqf Group of Oman. *Chem. Geol.* 111, 269–282. [http://dx.doi.org/10.1016/0009-2541\(94\)90094-9](http://dx.doi.org/10.1016/0009-2541(94)90094-9).
- Calver, C.R., 2000. Isotope stratigraphy of the Ediacaran (Neoproterozoic III) of the Adelaide Rift Complex, Australia, and the overprint of water column stratification. *Precambr. Res.* 100, 121–150. [http://dx.doi.org/10.1016/s0301-9268\(99\)00072-8](http://dx.doi.org/10.1016/s0301-9268(99)00072-8).
- Canfield, D.E., Teske, A., 1996. Late Proterozoic rise in atmospheric oxygen concentration inferred from phylogenetic and sulphur-isotope studies. *Nature* 382, 127–132. <http://dx.doi.org/10.1038/382127a0>.
- Claypool, G.E., Kaplan, I., 1974. The origin and distribution of methane in marine sediments. In: I.R., Kaplan (Ed.), *Natural Gases in Marine Sediments*. Springer, Boston, MA, pp. 99–139. http://dx.doi.org/10.1007/978-1-4684-2757-8_8.
- Crowe, S.A., Paris, G., Katsev, S., Jones, C., Kim, S.-T., Zerkle, A.L., Nomosatoryo, S., Fowle, D.A., Adkins, J.F., Sessions, A.L., 2014. Sulfate was a trace constituent of Archean seawater. *Science* 346, 735–739. <http://dx.doi.org/10.1126/science.1258966>.
- Cui, H., Kaufman, A.J., Xiao, S., Zhu, M., Liu, X.-M., 2015. Redox architecture of an Ediacaran ocean margin: integrated chemostratigraphic ($\delta^{13}\text{C}$ – $\delta^{34}\text{S}$ – $\delta^{87}\text{Sr}$ – $\delta^{86}\text{Sr}$ –Ce/Ce*) correlation of the Doushantuo Formation, South China. *Chem. Geol.* 405, 48–62. <http://dx.doi.org/10.1016/j.chemgeo.2015.04.009>.
- Cui, H., Grazhdankin, D.V., Xiao, S., Peek, S., Rogov, V.I., Bykova, N.V., Sievers, N.E., Liu, X.-M., Kaufman, A.J., 2016a. Redox-dependent distribution of early macro-organisms: Evidence from the terminal Ediacaran Khatyspyt Formation in Arctic Siberia. *Palaeogeogr. Palaeoclimatol. Palaeoecol.* 461, 122–139. <http://dx.doi.org/10.1016/j.palaeo.2016.08.015>.
- Cui, H., Kaufman, A.J., Xiao, S., Peek, S., Cao, H., Min, X., Cai, Y., Siegel, Z., Liu, X.M., Peng, Y., Schiffbauer, J.D., Martin, A.J., 2016b. Environmental context for the terminal Ediacaran biomineralization of animals. *Geobiology* 14, 344–363. <http://dx.doi.org/10.1111/gbi.12178>.
- Cui, H., Xiao, S., Zhou, C., Peng, Y., Kaufman, A.J., Plummer, R.E., 2016c. Phosphogenesis associated with the Shuram Excursion: petrographic and geochemical observations from the Ediacaran Doushantuo Formation of South China. *Sed. Geol.* 341, 134–146. <http://dx.doi.org/10.1016/j.sedgeo.2016.05.008>.
- Cui, H., 2017. Rock magnetic chronostratigraphy of the Shuram carbon isotope excursion: Wonoka Formation, Australia: COMMENT. *Geology* 45, e429. <http://dx.doi.org/10.1130/g39593c1>.
- Cui, H., Kaufman, A.J., Xiao, S., Zhou, C., Liu, X.-M., 2017. Was the Ediacaran Shuram Excursion a globally synchronized early diagenetic event? Insights from methane-derived authigenic carbonates in the uppermost Doushantuo Formation, South China. *Chem. Geol.* 450, 59–80. <http://dx.doi.org/10.1016/j.chemgeo.2016.12.010>.
- Day, E.S., James, N.P., Narbonne, G.M., Dalrymple, R., 2004. A sedimentary prelude to Marinoan glaciation, Cryogenian (Middle Neoproterozoic) Keele Formation, Mackenzie Mountains, northwestern Canada. *Precambr. Res.* 133, 223–247. <http://dx.doi.org/10.1016/j.precamres.2004.05.004>.
- Derry, L.A., Keto, L.S., Jacobsen, S.B., Knoll, A.H., Swett, K., 1989. Sr isotopic variations in Upper Proterozoic carbonates from Svalbard and East Greenland. *Geochim. Cosmochim. Acta* 53, 2331–2339. [http://dx.doi.org/10.1016/0016-7037\(89\)90355-4](http://dx.doi.org/10.1016/0016-7037(89)90355-4).
- Derry, L.A., Kaufman, A.J., Jacobsen, S.B., 1992. Sedimentary cycling and environmental change in the Late Proterozoic: evidence from stable and radiogenic isotopes. *Geochimica et Cosmochimica Acta* 56, 1317–1329. [http://dx.doi.org/10.1016/0016-7037\(92\)90064-p](http://dx.doi.org/10.1016/0016-7037(92)90064-p).
- Derry, L.A., 2010. A burial diagenesis origin for the Ediacaran Shuram-Wonoka carbon isotope anomaly. *Earth Planet. Sci. Lett.* 294, 152–162. <http://dx.doi.org/10.1016/j.epsl.2010.03.022>.
- Des Marais, D.J., Strauss, H., Summons, R.E., Hayes, J.M., 1992. Carbon isotope evidence for the stepwise oxidation of the Proterozoic environment. *Nature* 359, 605–609. <http://dx.doi.org/10.1038/359605a0>.
- Duda, J.-P., Zhu, M., Reitner, J., 2015. Depositional dynamics of a bituminous carbonate facies in a tectonically induced intra-platform basin: the Shibantan Member (Dengying Formation, Ediacaran Period). *Carb. Evap.* 31, 87–99. <http://dx.doi.org/10.1007/s13146-015-0243-8>.
- Eisbacher, G.H., 1985. Late proterozoic rifting, glacial sedimentation, and sedimentary cycles in the light of Windermere deposition, Western Canada. *Palaeogeogr. Palaeoclimatol. Palaeoecol.* 51, 231–254. [http://dx.doi.org/10.1016/0031-0182\(85\)90087-2](http://dx.doi.org/10.1016/0031-0182(85)90087-2).
- Fan, J., Peng, P.a., Melchin, M., 2009. Carbon isotopes and event stratigraphy near the Ordovician-Silurian boundary, Yichang, South China. *Palaeogeogr. Palaeoclimatol. Palaeoecol.* 276, 160–169. <http://dx.doi.org/10.1016/j.palaeo.2009.03.007>.
- Fike, D.A., Grotzinger, J.P., Pratt, L.M., Summons, R.E., 2006. Oxidation of the Ediacaran ocean. *Nature* 444, 744–747. <http://dx.doi.org/10.1038/nature05345>.
- Fike, D.A., Bradley, A.S., Rose, C.V., 2015. Rethinking the ancient sulfur cycle. *Annu. Rev. Earth Planet. Sci.* 43, 593–622. <http://dx.doi.org/10.1146/annurev-earth-060313-054802>.
- Frets, D.C., 1969. *Geology and Structure of the Huab-Welwitschia Area. University of Cape Town, Department of Geology, South West Africa*, pp. 235.
- Gao, Y., Zhang, X., Zhang, G., Chen, K., Shen, Y., 2018. Ediacaran negative C-isotopic excursions associated with phosphogenic events: Evidence from South China. *Precambr. Res.* 307, 218–228. <http://dx.doi.org/10.1016/j.precamres.2018.01.014>.
- Germs, G.J.B., 1995. The Neoproterozoic of southwestern Africa, with emphasis on platform stratigraphy and paleontology. *Precambr. Res.* 73, 137–151. [http://dx.doi.org/10.1016/s0031-9268\(94\)00075-3](http://dx.doi.org/10.1016/s0031-9268(94)00075-3).
- Gill, B.C., Lyons, T.W., Young, S.A., Kump, L.R., Knoll, A.H., Saltzman, M.R., 2011. Geochemical evidence for widespread euxinia in the Later Cambrian ocean. *Nature* 469, 80–83. <http://dx.doi.org/10.1038/nature09700>.
- Gischler, E., Swart, P.K., Lomando, A.J., 2007. Stable isotopes of carbon and oxygen in modern sediments of carbonate platforms, barrier reefs, atolls and ramps: patterns and implications. In: Swart, Peter K., Eberli, Gregor P., McKenzie, Judith A. (Eds.), *Perspectives in Carbonate Geology: A Tribute to the Career of Robert Nathan Ginsburg*, pp. 61–74. <http://dx.doi.org/10.1002/9781444312065.ch5>.
- Gomez, F.J., Kah, L.C., Bartley, J.K., Astini, R.A., 2014. Microbialites in a high-altitude Andean lake: multiple controls in carbonate precipitation and lamina accretion. *PALAIOS* 29, 233–249. <http://dx.doi.org/10.2110/palo.2013.049>.
- Gorjan, P., Veevers, J.J., Walter, M.R., 2000. Neoproterozoic sulfur-isotope variation in Australia and global implications. *Precambr. Res.* 100, 151–179. [http://dx.doi.org/10.1016/s0301-9268\(99\)00073-x](http://dx.doi.org/10.1016/s0301-9268(99)00073-x).
- Gorjan, P., Walter, M.R., Swart, R., 2003. Global Neoproterozoic (Sturtian) post-glacial sulfide-sulfur isotope anomaly recognised in Namibia. *J. Afr. Earth Sc.* 36, 89–98. [http://dx.doi.org/10.1016/S0899-5362\(03\)00002-2](http://dx.doi.org/10.1016/S0899-5362(03)00002-2).
- Grotzinger, J.P., Fike, D.A., Fischer, W.W., 2011. Enigmatic origin of the largest-known carbon isotope excursion in Earth's history. *Nat. Geosci.* 4, 285–292. <http://dx.doi.org/10.1038/ngeo1138>.
- Guacaneme, C., Babinski, M., Paula-Santos, G.M.D., Pedrosa-Soares, A.C., 2017. C, O, and

- Sr isotopic variations in Neoproterozoic-Cambrian carbonate rocks from Sete Lagoas Formation (Bambuí Group), in the Southern São Francisco Basin, Brazil. *Braz. J. Geol.* 47, 521–543. <http://dx.doi.org/10.1590/2317-4889201720160126>.
- Guan, C., Zhou, C., Wang, W., Wan, B., Yuan, X., Chen, Z., 2014. Fluctuation of shelf basin redox conditions in the early Ediacaran: evidence from Lantian Formation black shales in South China. *Precambr. Res.* 245, 1–12. <http://dx.doi.org/10.1016/j.precamres.2014.01.003>.
- Guo, X., Chafetz, H.S., 2014. Trends in ^{87}O and ^{81}C values in lacustrine tufa mounds: Palaeohydrology of Searles Lake, California. *Sedimentology* 61, 221–237. <http://dx.doi.org/10.1111/sed.12085>.
- Habicht, K.S., Gade, M., Thamdrup, B., Berg, P., Canfield, D.E., 2002. Calibration of sulfate levels in the Archean ocean. *Science* 298, 2372–2374. <http://dx.doi.org/10.1126/science.1078265>.
- Halverson, G.P., Hoffman, P.F., Schrag, D.P., Kaufman, A.J., 2002. A major perturbation of the carbon cycle before the Ghaub glaciation (Neoproterozoic) in Namibia: Prelude to snowball Earth? *Geochem. Geophys. Geosyst.* 3, 1–24. <http://dx.doi.org/10.1029/2001gc000244>.
- Halverson, G.P., Maloof, A.C., Hoffman, P.F., 2004. The Marinoan glaciation (Neoproterozoic) in northeast Svalbard. *Basin Res.* 16, 297–324. <http://dx.doi.org/10.1111/j.1365-2117.2004.00234.x>.
- Halverson, G.P., Hoffman, P.F., Schrag, D.P., Maloof, A.C., Rice, A.H.N., 2005. Toward a Neoproterozoic composite carbon-isotope record. *Geol. Soc. Am. Bull.* 117, 1181–1207. <http://dx.doi.org/10.1130/b25630.1>.
- Halverson, G.P., Dudás, F.Ö., Maloof, A.C., Bowring, S.A., 2007. Evolution of the $^{87}\text{Sr}/^{86}\text{Sr}$ composition of Neoproterozoic seawater. *Palaeogeogr. Palaeoclimatol. Palaeoecol.* 256, 103–129. <http://dx.doi.org/10.1016/j.palaeo.2007.02.028>.
- Halverson, G.P., Wade, B.P., Hurtgen, M.T., Barovich, K.M., 2010. Neoproterozoic chemostratigraphy. *Precambr. Res.* 182, 337–350. <http://dx.doi.org/10.1016/j.precamres.2010.04.007>.
- Halverson, G.P., Shields-Zhou, G., 2011. Chemostratigraphy and the Neoproterozoic glaciations. Memoirs In: Arnaud, E., Halverson, G.P., Shields-Zhou, G. (Eds.), *The Geological Record of Neoproterozoic Glaciations*. Geological Society, London, pp. 51–66. <http://dx.doi.org/10.1144/m36.4>.
- Hayes, J.M., Lambert, I.B., Strauss, H., 1992. The sulfur-isotopic record. In: Schopf, J.W., Klein, C. (Eds.), *The Proterozoic Biosphere: A Multidisciplinary Study*. Cambridge University Press, Cambridge, pp. 129–132.
- Hayes, J.M., Strauss, H., Kaufman, A.J., 1999. The abundance of ^{13}C in marine organic matter and isotopic fractionation in the global biogeochemical cycle of carbon during the past 800 Ma. *Chem. Geol.* 161, 103–125. [http://dx.doi.org/10.1016/s0009-2541\(99\)00083-2](http://dx.doi.org/10.1016/s0009-2541(99)00083-2).
- Hayes, J.M., Waldbauer, J.R., 2006. The carbon cycle and associated redox processes through time. *Philos. Trans. R. Soc. B* 361, 931–950. <http://dx.doi.org/10.1098/rstb.2006.1840>.
- Higgins, J., Fischer, W., Schrag, D., 2009. Oxygenation of the ocean and sediments: consequences for the seafloor carbonate factory. *Earth Planet. Sci. Lett.* 284, 25–33. <http://dx.doi.org/10.1016/j.epsl.2009.03.039>.
- Hoffman, P.F., Kaufman, A.J., Halverson, G.P., 1998a. Comings and goings of global glaciations on a Neoproterozoic tropical platform in Namibia. *GSA Today* 8, 1–9.
- Hoffman, P.F., Kaufman, A.J., Halverson, G.P., Schrag, D.P., 1998b. Neoproterozoic Snowball Earth. *Science* 281, 1342–1346. <http://dx.doi.org/10.1126/science.281.5381.1342>.
- Hoffman, P.F., Halverson, G.P., Domack, E.W., Husson, J.M., Higgins, J.A., Schrag, D.P., 2007. Are basal Ediacaran (635 Ma) post-glacial “cap dolostones” diachronous? *Earth Planet. Sci. Lett.* 258, 114–131. <http://dx.doi.org/10.1016/j.epsl.2007.03.032>.
- Hoffman, P.F., 2011. Strange bedfellows: glacial diamictite and cap carbonate from the Marinoan (635 Ma) glaciation in Namibia. *Sedimentology* 58, 57–119. <http://dx.doi.org/10.1111/j.1365-3091.2010.01206.x>.
- Hoffman, P.F., Lamothe, K.G., LoBianco, S.J.C., Hodgskiss, M.S.W., Bellefroid, E.J., Johnson, B.W., Hodgin, E.B., Halverson, G.P., 2017. Sedimentary depocenters on Snowball Earth: case studies from the Sturtian Chus Formation in northern Namibia. *Geosphere* 13, 811–837. <http://dx.doi.org/10.1130/ges01457.1>.
- Hoffman, P.F., Halverson, G.P., 2018. Discussion of “Depositional ages and provenance of the Neoproterozoic Damara Supergroup (northwest Namibia): Implications for the Angola-Congo and Kalahari cratons connection” by Débora B. Nascimento, Renata S. Schmitt, André Ribeiro, Rudolph A. J. Trouw, Cees W. Passchier, and Miguel A. S. Basei. *Gondwana Research*, 58, 235–238. <https://doi.org/10.1016/j.gr.2018.02.003>.
- Hoffmann, K.-H., Prave, A.R., 1996. A preliminary note on a revised subdivision and regional correlation of the Otavi Group based on glaciogenic diamictites and associated cap dolostones. *Commun. Geol. Surv. Namibia* 11, 83–88.
- Holser, W.T., Schidlowski, M., Mackenzie, F.T., Maynard, J.B., 1988. Geochemical Cycles of Carbon and Sulfur. In: Gregor, C.B., Garrels, R.M., Mackenzie, F.T., Barry, M.J. (Eds.), *Chemical Cycles in the Evolution of the Earth*. Wiley-Interscience, New York, pp. 105–173.
- Horton, T.W., Deffeyes, W.F., Tripati, A.K., Oze, C., 2015. Evaporation induced ^{18}O and ^{13}C enrichment in lake systems: a global perspective on hydrologic balance effects. *Quat. Sci. Rev.* 365–379. <http://dx.doi.org/10.1016/j.quascirev.2015.06.030>.
- Husson, J.M., Maloof, A.C., Schoene, B., Chen, C.Y., Higgins, J.A., 2015. Stratigraphic expression of Earth’s deepest ^{81}C excursion in the Wonoka Formation of South Australia. *Am. J. Sci.* 315, 1–45. <http://dx.doi.org/10.2475/01.2015.01>.
- Irwin, H., Curtis, C., Coleman, M., 1977. Isotopic evidence for source of diagenetic carbonates formed during burial of organic-rich sediments. *Nature* 269, 209–213. <http://dx.doi.org/10.1038/269209a0>.
- Iyer, S.S., Babinski, M., Krouse, H.R., Chemale Jr, F., 1995. Highly ^{13}C -enriched carbonate and organic matter in the Neoproterozoic sediments of the Bambuí Group, Brazil. *Precambr. Res.* 73, 271–282. [http://dx.doi.org/10.1016/0301-9268\(94\)00082-3](http://dx.doi.org/10.1016/0301-9268(94)00082-3).
- Jacobsen, S.B., Kaufman, A.J., 1999. The Sr, C and O isotopic evolution of Neoproterozoic seawater. *Chem. Geol.* 161, 37–57. [http://dx.doi.org/10.1016/s0009-2541\(99\)00080-7](http://dx.doi.org/10.1016/s0009-2541(99)00080-7).
- James, N.P., Narbonne, G.M., Kyser, T.K., 2001. Late Neoproterozoic cap carbonates: Mackenzie Mountains, northwestern Canada: precipitation and global glacial melt-down. *Can. J. Earth Sci.* 38, 1229–1262. <http://dx.doi.org/10.1139/cjes-38-8-1229>.
- Jiang, G., Kaufman, A.J., Christie-Blick, N., Zhang, S., Wu, H., 2007. Carbon isotope variability across the Ediacaran Yangtze platform in South China: Implications for a large surface-to-deep ocean ^{81}C gradient. *Earth Planet. Sci. Lett.* 261, 303–320. <http://dx.doi.org/10.1016/j.epsl.2007.07.009>.
- Jones, D.S., Fike, D.A., 2013. Dynamic sulfur and carbon cycling through the end-Ordovician extinction revealed by paired sulfate–pyrite ^{34}S . *Earth Planet. Sci. Lett.* 363, 144–155. <http://dx.doi.org/10.1016/j.epsl.2012.12.015>.
- Karhu, J.A., Holland, H.D., 1996. Carbon isotopes and the rise of atmospheric oxygen. *Geology* 24, 867–870. [http://dx.doi.org/10.1130/0091-7613\(1996\)024<0867:ciatro>2.3.co;2](http://dx.doi.org/10.1130/0091-7613(1996)024<0867:ciatro>2.3.co;2).
- Kasemann, S.A., Pogge von Strandmann, P.A., Prave, A.R., Fallick, A.E., Elliott, T., Hoffmann, K.-H., 2014. Continental weathering following a Cryogenian glaciation: Evidence from calcium and magnesium isotopes. *Earth Planet. Sci. Lett.* 396, 66–77. <http://dx.doi.org/10.1016/j.epsl.2014.03.048>.
- Kaufman, A.J., Hayes, J.M., Knoll, A.H., Germs, G.J.B., 1991. Isotopic compositions of carbonates and organic carbon from upper Proterozoic successions in Namibia: stratigraphic variation and the effects of diagenesis and metamorphism. *Precambr. Res.* 49, 301–327. [http://dx.doi.org/10.1016/0301-9268\(91\)90039-d](http://dx.doi.org/10.1016/0301-9268(91)90039-d).
- Kaufman, A.J., Jacobsen, S.B., Knoll, A.H., 1993. The Vendian record of Sr and C isotopic variations in seawater: implications for tectonics and paleoclimate. *Earth Planet. Sci. Lett.* 120, 409–430. [http://dx.doi.org/10.1016/0012-821x\(93\)90254-7](http://dx.doi.org/10.1016/0012-821x(93)90254-7).
- Kaufman, A.J., Knoll, A.H., 1995. Neoproterozoic variations in the C-isotopic composition of seawater: stratigraphic and biogeochemical implications. *Precambr. Res.* 73, 27–49. [http://dx.doi.org/10.1016/0301-9268\(94\)00070-8](http://dx.doi.org/10.1016/0301-9268(94)00070-8).
- Kaufman, A.J., Knoll, A.H., Narbonne, G.M., 1997. Isotopes, ice ages, and terminal Proterozoic earth history. *Proc. Natl. Acad. Sci.* 94, 6600–6605.
- Kaufman, A.J., Corsetti, F.A., Varni, M.A., 2007. The effect of rising atmospheric oxygen on carbon and sulfur isotope anomalies in the Neoproterozoic Johnnie Formation, Death Valley, USA. *Chem. Geol.* 237, 47–63. <http://dx.doi.org/10.1016/j.chemgeo.2006.06.023>.
- Kaufman, A.J., Sial, A.N., Frimmel, H.E., Misi, A., 2009. Neoproterozoic to Cambrian palaeoclimatic events in southwestern Gondwana. In: Gaucher, C., Sial, A.N., Halverson, G.P., Frimmel, H.E. (Eds.), *Neoproterozoic-Cambrian Tectonics, Global Change and Evolution: a focus on southwestern Gondwana*. Developments in Precambrian Geology, Elsevier, Amsterdam, Netherlands, pp. 369–388. [http://dx.doi.org/10.1016/s0166-2635\(09\)01626-0](http://dx.doi.org/10.1016/s0166-2635(09)01626-0).
- Kennedy, M.J., Runnegar, B., Prave, A.R., Hoffmann, K.-H., Arthur, M.A., 1998. Two or four Neoproterozoic glaciations? *Geology* 26, 1059–1063. [http://dx.doi.org/10.1130/0091-7613\(1998\)026<1059:tnofng>2.3.co;2](http://dx.doi.org/10.1130/0091-7613(1998)026<1059:tnofng>2.3.co;2).
- Klaebe, R.M., Kennedy, M.J., Jarrett, A.J.M., Brocks, J.J., 2016. Local paleoenvironmental controls on the carbon-isotope record defining the Bitter Springs Anomaly. *Geobiology* 15, 65–80. <http://dx.doi.org/10.1111/gbi.12217>.
- Knauth, L.P., Kennedy, M.J., 2009. The late Precambrian greening of the Earth. *Nature* 460, 728–732. <http://dx.doi.org/10.1038/nature08213>.
- Knoll, A.H., Hayes, J.M., Kaufman, A.J., Swett, K., Lambert, I.B., 1986. Secular variation in carbon isotope ratios from Upper Proterozoic successions of Svalbard and East Greenland. *Nature* 321, 832–838. <http://dx.doi.org/10.1038/321832a0>.
- Knoll, A.H., Grotzinger, J.P., Kaufman, A.J., Kolosov, P., 1995. Integrated approaches to terminal Proterozoic stratigraphy: an example from the Olenek Uplift, northeastern Siberia. *Precambr. Res.* 73, 251–270. [http://dx.doi.org/10.1016/0301-9268\(94\)00081-2](http://dx.doi.org/10.1016/0301-9268(94)00081-2).
- Kump, L., Arthur, M., Patzkowsky, M., Gibbs, M., Pinkus, D., Sheehan, P., 1999. A weathering hypothesis for glaciation at high atmospheric pCO₂ during the Late Ordovician. *Palaeogeogr. Palaeoclimatol. Palaeoecol.* 152, 173–187. [http://dx.doi.org/10.1016/S0031-0182\(99\)00046-2](http://dx.doi.org/10.1016/S0031-0182(99)00046-2).
- Kump, L.R., Arthur, M.A., 1999. Interpreting carbon-isotope excursions: carbonates and organic matter. *Chem. Geol.* 161, 181–198. [http://dx.doi.org/10.1016/s0009-2541\(99\)00086-8](http://dx.doi.org/10.1016/s0009-2541(99)00086-8).
- Lechner, M., Pogge von Strandmann, P.A.E., Jenkyns, H.C., Prosser, G., Parente, M., 2015. Lithium-isotope evidence for enhanced silicate weathering during OAE 1a (Early Aptian Selli event). *Earth Planet. Sci. Lett.* 432, 210–222. <http://dx.doi.org/10.1016/j.epsl.2015.09.052>.
- Lee, C., Fike, D.A., Love, G.D., Sessions, A.L., Grotzinger, J.P., Summons, R.E., Fischer, W.W., 2013. Carbon isotopes and lipid biomarkers from organic-rich facies of the Shuram Formation, Sultanate of Oman. *Geobiology* 11, 406–419. <http://dx.doi.org/10.1111/gbi.12045>.
- Li, H.C., Ku, T.L., 1997. ^{13}C – ^{18}O covariance as a paleohydrological indicator for closed-basin lakes. *Palaeogeogr. Palaeoclimatol. Palaeoecol.* 133, 69–80. [http://dx.doi.org/10.1016/S0031-0182\(96\)00153-8](http://dx.doi.org/10.1016/S0031-0182(96)00153-8).
- Ling, H.-F., Chen, X., Li, D., Wang, D., Shields-Zhou, G.A., Zhu, M., 2013. Cerium anomaly variations in Ediacaran–earliest Cambrian carbonates from the Yangtze Gorges area, South China: Implications for oxygenation of coeval shallow seawater. *Precambr. Res.* 225, 110–127. <http://dx.doi.org/10.1016/j.precamres.2011.10.011>.
- Lu, M., Zhu, M., Zhang, J., Shields-Zhou, G., Li, G., Zhao, F., Zhao, X., Zhao, M., 2013. The DOUNCE event at the top of the Ediacaran Doushantuo Formation, South China: Broad stratigraphic occurrence and non-diagenetic origin. *Precambr. Res.* 225, 86–109. <http://dx.doi.org/10.1016/j.precamres.2011.10.018>.
- Macdonald, F.A., Jones, D.S., Schrag, D.P., 2009. Stratigraphic and tectonic implications of a newly discovered glacial diamictite-cap carbonate couplet in southwestern Mongolia. *Geology* 37, 123–126. <http://dx.doi.org/10.1130/g24797a.1>.
- Macdonald, F.A., Strauss, J.V., Sperling, E.A., Halverson, G.P., Narbonne, G.M., Johnston,

- D.T., Kunzmann, M., Schrag, D.P., Higgins, J.A., 2013. The stratigraphic relationship between the Shuram carbon isotope excursion, the oxygenation of Neoproterozoic oceans, and the first appearance of the Ediacara biota and bilaterian trace fossils in northwestern Canada. *Chem. Geol.* 362, 250–272. <http://dx.doi.org/10.1016/j.chemgeo.2013.05.032>.
- Martin, A.P., Condon, D.J., Prave, A.R., Lepland, A., 2013. A review of temporal constraints for the Palaeoproterozoic large, positive carbonate carbon isotope excursion (the Lomagundi-Jatuli Event). *Earth Sci. Rev.* 127, 242–261. <http://dx.doi.org/10.1016/j.earscirev.2013.10.006>.
- McFadden, K.A., Huang, J., Chu, X., Jiang, G., Kaufman, A.J., Zhou, C., Yuan, X., Xiao, S., 2008. Pulsed oxidation and biological evolution in the Ediacaran Doushantuo Formation. *Proc. Natl. Acad. Sci.* 105, 3197–3202. <http://dx.doi.org/10.1073/pnas.0708336105>.
- McKirdy, D.M., Burgess, J.M., Lemon, N.M., Yu, X., Cooper, A.M., Gostin, V.A., Jenkins, R.J.F., Both, R.A., 2001. A chemostratigraphic overview of the late Cryogenian interglacial sequence in the Adelaide Fold-Thrust Belt, South Australia. *Precambr. Res.* 106, 149–186. [http://dx.doi.org/10.1016/S0301-9268\(00\)00130-3](http://dx.doi.org/10.1016/S0301-9268(00)00130-3).
- Meister, P., McKenzie, J.A., Vasconcelos, C., Bernasconi, S., Frank, M., Gutjahr, M., Schrag, D.P., 2007. Dolomite formation in the dynamic deep biosphere: results from the Peru Margin. *Sedimentology* 54, 1007–1032. <http://dx.doi.org/10.1111/j.1365-3091.2007.00870.x>.
- Melchin, M.J., Holmden, C., 2006. Carbon isotope chemostratigraphy in Arctic Canada: sea-level forcing of carbonate platform weathering and implications for Hirnantian global correlation. *Palaeogeogr. Palaeoclimatol. Palaeoecol.* 234, 186–200. <http://dx.doi.org/10.1016/j.palaeo.2005.10.009>.
- Melezhik, V.A., Pokrovsky, B.G., Fallick, A.E., Kuznetsov, A.B., Bujakaite, M.I., 2009. Constraints on $^{87}\text{Sr}/^{86}\text{Sr}$ of Late Ediacaran seawater: insight from Siberian high-Sr limestones. *J. Geol. Soc.* 166, 183–191. <http://dx.doi.org/10.1144/0016-76492007-171>.
- Miller, R.M., 2013. Comparative stratigraphic and geochronological evolution of the Northern Damara Supergroup in Namibia and the Katanga Supergroup in the Lufilian Arc of Central Africa. *Geosci. Can.* 40, 118–140. <https://doi.org/10.12789/geocanj.2013.40.007>.
- Misi, A., Veizer, J., 1998. Neoproterozoic carbonate sequences of the Una Group, Irecê Basin, Brazil: chemostratigraphy, age and correlations. *Precambr. Res.* 89, 87–100. [http://dx.doi.org/10.1016/S0301-9268\(97\)00073-9](http://dx.doi.org/10.1016/S0301-9268(97)00073-9).
- Misi, A., Kaufman, A.J., Veizer, J., Powis, K., Azmy, K., Boggiani, P.C., Gaucher, C., Teixeira, J.B.G., Sanches, A.L., Iyer, S.S., 2007. Chemostratigraphic correlation of Neoproterozoic successions in South America. *Chem. Geol.* 237, 143–167. <http://dx.doi.org/10.1016/j.chemgeo.2006.06.019>.
- Misra, S., Froelich, P.N., 2012. Lithium isotope history of cenozoic seawater: changes in silicate weathering and reverse weathering. *Science* 335, 818–823. <http://dx.doi.org/10.1126/science.1214697>.
- Narbonne, G.M., Kaufman, A.J., Knoll, A.H., 1994. Integrated chemostratigraphy and biostratigraphy of the Windermere Supergroup, northwestern Canada: Implications for Neoproterozoic correlations and the early evolution of animals. *Geol. Soc. Am. Bull.* 106, 1281–1292. [http://dx.doi.org/10.1130/0016-7606\(1994\)106<1281:icabot>2.3.co;2](http://dx.doi.org/10.1130/0016-7606(1994)106<1281:icabot>2.3.co;2).
- Narbonne, G.M., Aitken, J.D., 1995. Neoproterozoic of the Mackenzie Mountains, northwestern Canada. *Precambr. Res.* 73, 101–121. [http://dx.doi.org/10.1016/S0301-9268\(94\)00073-Z](http://dx.doi.org/10.1016/S0301-9268(94)00073-Z).
- Narbonne, G.M., Xiao, S., Shields, G.A., Gehling, J.G., 2012. The Ediacaran period. In: Gradstein, F.M., Ogg, J.G., Schmitz, M.D., Ogg, G.M. (Eds.), *The Geologic Time Scale*. Elsevier, Boston, USA, pp. 413–435. <http://dx.doi.org/10.1016/b978-0-444-59425-9.00018-4>.
- Nascimento, D.B., Schmitt, R.S., Ribeiro, A., Trouw, R.A.J., Passchier, C.W., Basei, M.A.S., 2017. Depositional ages and provenance of the Neoproterozoic Damara Supergroup (northwest Namibia): Implications for the Angola-Congo and Kalahari cratons connection. *Gondwana Res.* 52, 153–171. <http://dx.doi.org/10.1016/j.gr.2017.09.006>.
- Nascimento, D.B., Ribeiro, A., Trouw, R.A.J., Schmitt, R.S., Passchier, C.W., 2018. Reply to discussion by Hoffman and Halverson (2018) on the article: “Depositional ages and provenance of the Neoproterozoic Damara Supergroup: (northwest Namibia): Implications for the Angola-Congo and Kalahari cratons connection” by Nascimento et al. (2017). *Gondwana Research*, 52, 153–171. *Gondwana Research*, 58, 239–240. <https://doi.org/10.1016/j.gr.2018.02.004>.
- Oehlert, A.M., Swart, P.K., 2014. Interpreting carbonate and organic carbon isotope covariance in the sedimentary record. *Nat. Commun.* 5, 4672. <http://dx.doi.org/10.1038/ncomms5672>.
- Ossa Ossa, F., Eickmann, B., Hofmann, A., Planavsky, N.J., Asael, D., Pambo, F., Bekker, A., 2018. Two-step deoxygenation at the end of the Paleoproterozoic Lomagundi Event. *Earth Planet. Sci. Lett.* 486, 70–83. <http://dx.doi.org/10.1016/j.epsl.2018.01.009>.
- Paula-Santos, G.M., Babinski, M., Kuchenbecker, M., Caetano-Filho, S., Trindade, R.I., Pedrosa-Soares, A.C., 2015. New evidence of an Ediacaran age for the Bambuí Group in southern São Francisco craton (eastern Brazil) from zircon U-Pb data and isotope chemostratigraphy. *Gondwana Res.* 28, 702–720. <http://dx.doi.org/10.1016/j.gr.2014.07.012>.
- Paula-Santos, G.M., Caetano-Filho, S., Babinski, M., Trindade, R.I., Guacaneme, C., 2017. Tracking connection and restriction of West Gondwana São Francisco Basin through isotope chemostratigraphy. *Gondwana Res.* 42, 280–305. <http://dx.doi.org/10.1016/j.gr.2016.10.012>.
- Pierre, C., Blanc-Valleron, M.M., Caquineau, S., März, C., Ravelo, A.C., Takahashi, K., Alvarez Zarikian, C., 2016. Mineralogical, geochemical and isotopic characterization of authigenic carbonates from the methane-bearing sediments of the Bering Sea continental margin (IODP Expedition 323, Sites U1343–U1345). *Deep Sea Res. Part II* 125–126, 133–144. <http://dx.doi.org/10.1016/j.dsr2.2014.03.011>.
- Planavsky, N.J., Bekker, A., Hofmann, A., Owens, J.D., Lyons, T.W., 2012. Sulfur record of rising and falling marine oxygen and sulfate levels during the Lomagundi event. *Proc. Natl. Acad. Sci.* 109, 18300–18305. <http://dx.doi.org/10.1073/pnas.1120387109>.
- Pokrovsky, B.G., Mavromatis, V., Pokrovsky, O.S., 2011. Co-variation of Mg and C isotopes in late Precambrian carbonates of the Siberian Platform: A new tool for tracing the change in weathering regime? *Chem. Geol.* 290, 67–74. <http://dx.doi.org/10.1016/j.chemgeo.2011.08.015>.
- Pope, M.C., Grotzinger, J.P., 2003. Paleoproterozoic Stark Formation, Athabasca basin, northwest Canada: Record of cratonic-scale salinity crisis. *J. Sediment. Res.* 73, 280–295. <http://dx.doi.org/10.1306/091302730280>.
- Prave, A.R., Condon, D.J., Hoffmann, K.H., Tapster, S., Fallick, A.E., 2016. Duration and nature of the end-Cryogenian (Marinoan) glaciation. *Geology* 44, 631–634. <http://dx.doi.org/10.1130/g38089.1>.
- Ripperdan, R.L., 2001. Stratigraphic variation in marine carbonate carbon isotope ratios. In: Valley, J.W., Cole, D.R. (Eds.), *Reviews in Mineralogy and Geochemistry: Stable Isotope Geochemistry*. The Mineralogical Society Of America, Washington, D.C., pp. 637–662. <http://dx.doi.org/10.2138/gsmg.43.1.637>.
- Rose, C.V., Swanson-Hysell, N.L., Husson, J.M., Popick, L.N., Cottle, J.M., Schoene, B., Maloof, A.C., 2012. Constraints on the origin and relative timing of the Trezona ^{81}C anomaly below the end-Cryogenian glaciation. *Earth Planet. Sci. Lett.* 319–320, 241–250. <http://dx.doi.org/10.1016/j.epsl.2011.12.027>.
- Sahoo, S.K., Planavsky, N.J., Kendall, B., Wang, X., Shi, X., Scott, C., Anbar, A.D., Lyons, T.W., Jiang, G., 2012. Ocean oxygenation in the wake of the Marinoan glaciation. *Nature* 489, 546–549. <http://dx.doi.org/10.1038/nature11445>.
- Sahoo, S.K., 2015. *Ediacaran Ocean Redox Evolution*. Ph.D. dissertation. University of Nevada, Las Vegas, pp. 191.
- Sahoo, S.K., Planavsky, N.J., Jiang, G., Kendall, B., Owens, J.D., Wang, X., Shi, X., Anbar, A.D., Lyons, T.W., 2016. Oceanic oxygenation events in the anoxic Ediacaran ocean. *Geobiology* 14, 457–468. <http://dx.doi.org/10.1111/gbi.12182>.
- Saltzman, M.R., Thomas, E., 2012. Carbon isotope stratigraphy. In: Gradstein, F.M., Ogg, J.G., Schmitz, M.D., Ogg, G.M. (Eds.), *The Geologic Time Scale*. Elsevier, Boston, USA, pp. 207–232. <http://dx.doi.org/10.1016/b978-0-444-59425-9.00011-1>.
- Sawaki, Y., Ohno, T., Tahata, M., Komiya, T., Hirata, T., Maruyama, S., Windley, B.F., Han, J., Shu, D., Li, Y., 2010. The Ediacaran radiogenic Sr isotope excursion in the Doushantuo Formation in the Three Gorges area, South China. *Precambr. Res.* 176, 46–64. <http://dx.doi.org/10.1016/j.precamres.2009.10.006>.
- Saylor, B.Z., Kaufman, A.J., Grotzinger, J.P., Urban, F., 1998. A composite reference section for terminal Proterozoic strata of southern Namibia. *J. Sediment. Res.* 68, 1223–1235. <http://dx.doi.org/10.2110/jsr.68.1223>.
- Schidlowski, M., Eichmann, R., Junge, C.E., 1976. Carbon isotope geochemistry of the Precambrian Lomagundi carbonate province, Rhodesia. *Geochim. Cosmochim. Acta* 40, 449–455. [http://dx.doi.org/10.1016/0016-7037\(76\)90010-7](http://dx.doi.org/10.1016/0016-7037(76)90010-7).
- Schidlowski, M., Matzkiegut, U., Krumbine, W.E., 1984. Superheavy organic carbon from hypersaline microbial mats. *Naturwissenschaften* 71, 303–308. <http://dx.doi.org/10.1007/bf00396613>.
- Schrag, D.P., Higgins, J.A., Macdonald, F.A., Johnston, D.T., 2013. Authigenic carbonate and the history of the global carbon cycle. *Science* 339, 540–543. <http://dx.doi.org/10.1126/science.1229578>.
- Shields-Zhou, G.A., Hill, A.C., Macgbahann, B.A., 2012. The cryogenian period. In: Gradstein, F.M., Ogg, J.G., Schmitz, M.D., Ogg, G.M. (Eds.), *The Geologic Time Scale*. Elsevier, Boston, USA, pp. 393–411. <http://dx.doi.org/10.1016/b978-0-444-59425-9.00017-2>.
- Shields, G., Stille, P., Brasier, M.D., Atudorei, N.V., 1997. Stratified oceans and oxygenation of the late Precambrian environment: a post glacial geochemical record from the Neoproterozoic of W. Mongolia. *Terra Nova* 9, 218–222. <http://dx.doi.org/10.1111/j.1365-3121.1997.tb00016.x>.
- Shields, G.A., Brasier, M.D., Stille, P., Dorjnamjaa, D.-I., 2002. Factors contributing to high ^{81}C values in Cryogenian limestones of western Mongolia. *Earth Planet. Sci. Lett.* 196, 99–111. [http://dx.doi.org/10.1016/s0012-821x\(02\)00461-2](http://dx.doi.org/10.1016/s0012-821x(02)00461-2).
- Shields, G.A., 2017. Earth system transition during the Tonian–Cambrian interval of biological innovation: nutrients, climate, oxygen and the marine organic carbon capacitor. *Special Publications In: Brasier, A.T., McIlroy, D., McLoughlin, N. (Eds.), Earth System Evolution and Early Life: A Celebration of the Work of Martin Brasier*. Geological Society, London, pp. 161–177. <http://dx.doi.org/10.1144/sp448.17>.
- Shields, G.A., Mills, B.J.W., 2017. Tectonic controls on the long-term carbon isotope mass balance. *Proc. Natl. Acad. Sci.* 114, 4318–4323. <http://dx.doi.org/10.1073/pnas.1614506114>.
- Stiller, M., Rounick, J.S., Shasha, S., 1985. Extreme carbon-isotope enrichments in evaporating brines. *Nature* 316, 434–435. <http://dx.doi.org/10.1038/316434a0>.
- Strauss, H., 1993. The sulfur isotopic record of Precambrian sulfates: new data and a critical evaluation of the existing record. *Precambr. Res.* 63, 225–246. [http://dx.doi.org/10.1016/0301-9268\(93\)90035-z](http://dx.doi.org/10.1016/0301-9268(93)90035-z).
- Summons, R.E., Hayes, J.M., 1992. *Principles of molecular and isotopic biogeochemistry*. In: Schopf, J.W., Klein, C. (Eds.), *The Proterozoic Biosphere: A Multidisciplinary Study*. Cambridge University Press, Cambridge, pp. 83–93.
- Swanson-Hysell, N.L., Rose, C.V., Calmet, C.C., Halversen, G.P., Hurtgen, M.T., Maloof, A.C., 2010. Cryogenian glaciation and the onset of carbon-isotope decoupling. *Science* 328, 608–611. <http://dx.doi.org/10.1126/science.1184508>.
- Tahata, M., Ueno, Y., Ishikawa, T., Sawaki, Y., Murakami, K., Han, J., Shu, D., Li, Y., Guo, J., Yoshida, N., Komiya, T., 2013. Carbon and oxygen isotope chemostratigraphies of the Yangtze platform, South China: decoding temperature and environmental changes through the Ediacaran. *Gondwana Res.* 23, 333–353. <http://dx.doi.org/10.1016/j.gr.2012.04.005>.
- Talbot, M., Kelts, K., 1986. Primary and diagenetic carbonates in the anoxic sediments of Lake Bosumtwi, Ghana. *Geology* 14, 912–916. <http://dx.doi.org/10.1130/0091-934X-14-12-912>.

- Talbot, M., 1990. A review of the palaeohydrological interpretation of carbon and oxygen isotopic ratios in primary lacustrine carbonates. *Chem. Geol.* 80, 261–279. [http://dx.doi.org/10.1016/0168-9622\(90\)90009-2](http://dx.doi.org/10.1016/0168-9622(90)90009-2).
- Uhlen, G.J., Uhlein, A., Halverson, G.P., Stevenson, R., Caxito, F.A., Cox, G.M., Carvalho, J.F.M.G., 2016. The Carrancas Formation, Bambuí Group: a record of pre-Marinoan sedimentation on the southern São Francisco craton, Brazil. *J. S. Am. Earth Sci.* 71, 1–16. <http://dx.doi.org/10.1016/j.jsames.2016.06.009>.
- Valero-Garcés, B.L., Delgado-Huertas, A., Ratto, N., Navas, A., 1999. Large $\delta^{13}\text{C}$ enrichment in primary carbonates from Andean Altiplano lakes, northwest Argentina. *Earth Planet. Sci. Lett.* 171, 253–266. [http://dx.doi.org/10.1016/S0012-821X\(99\)00150-8](http://dx.doi.org/10.1016/S0012-821X(99)00150-8).
- Weizer, J., Compton, W., 1976. $^{87}\text{Sr}/^{86}\text{Sr}$ in Precambrian carbonates as an index of crustal evolution. *Geochim. Cosmochim. Acta* 40, 905–914. [http://dx.doi.org/10.1016/0016-7037\(76\)90139-3](http://dx.doi.org/10.1016/0016-7037(76)90139-3).
- Verdel, C., Wernicke, B.P., Bowring, S.A., 2011. The Shuram and subsequent Ediacaran carbon isotope excursions from southwest Laurentia, and implications for environmental stability during the metazoan radiation. *Geol. Soc. Am. Bull.* 123, 1539–1559. <http://dx.doi.org/10.1130/B30369.1>.
- Verdel, C., Campbell, M., 2017. Neoproterozoic carbon isotope stratigraphy of the Amadeus Basin, central Australia. *GSA Bulletin* 129, 1280–1299. <http://dx.doi.org/10.1130/B31562.1>.
- von Strandmann, P.A.P., Jenkyns, H.C., Woodfine, R.G., 2013. Lithium isotope evidence for enhanced weathering during Oceanic Anoxic Event 2. *Nat. Geosci.* 6, 668–672. <http://dx.doi.org/10.1038/ngeo1875>.
- Walter, M.R., Veevers, J.J., Calver, C.R., Gorjan, P., Hill, A.C., 2000. Dating the 840–544 Ma Neoproterozoic interval by isotopes of strontium, carbon, and sulfur in seawater, and some interpretative models. *Precambr. Res.* 100, 371–433. [http://dx.doi.org/10.1016/s0301-9268\(99\)00082-0](http://dx.doi.org/10.1016/s0301-9268(99)00082-0).
- Wan, B., Yuan, X., Chen, Z., Guan, C., Pang, K., Tang, Q., Xiao, S., 2016. Systematic description of putative animal fossils from the early Ediacaran Lantian Formation of South China. *Palaeontology* 59, 515–532. <http://dx.doi.org/10.1111/pala.12242>.
- Wang, W., Zhou, C., Yuan, X., Chen, Z., Xiao, S., 2012. A pronounced negative $\delta^{13}\text{C}$ excursion in an Ediacaran succession of western Yangtze Platform: a possible equivalent to the Shuram event and its implication for chemostratigraphic correlation in South China. *Gondwana Res.* 22, 1091–1101. <http://dx.doi.org/10.1016/j.gr.2012.02.017>.
- Wang, X., Jiang, G., Shi, X., Xiao, S., 2016. Paired carbonate and organic carbon isotope variations of the Ediacaran Doushantuo Formation from an upper slope section at Siduping, South China. *Precambr. Res.* 273, 53–66. <http://dx.doi.org/10.1016/j.precamres.2015.12.010>.
- Wehrmann, L.M., Risgaard-Petersen, N., Schrum, H.N., Walsh, E.A., Huh, Y., Ikebara, M., Pierre, C., D'Hondt, S., Ferdinand, T.G., Ravelo, A.C., Takahashi, K., Zarikian, C.A., 2011. Coupled organic and inorganic carbon cycling in the deep subseafloor sediment of the northeastern Bering Sea Slope (IODP Exp. 323). *Chem. Geol.* 284, 251–261. <http://dx.doi.org/10.1016/j.chemgeo.2011.03.002>.
- Wood, R.A., Poulton, S.W., Prave, A.R., Hoffmann, K.H., Clarkson, M.O., Guilbaud, R., Lyne, J.W., Tostevin, R., Bowyer, F., Penny, A.M., Curtis, A., Kasemann, S.A., 2015. Dynamic redox conditions control late Ediacaran metazoan ecosystems in the Nama Group, Namibia. *Precambr. Res.* 261, 252–271. <http://dx.doi.org/10.1016/j.precamres.2015.02.004>.
- Xiao, S., Narbonne, G.M., Zhou, C., Laflamme, M., Grazhdankin, D.V., Moczydłowska-Vidal, M., Cui, H., 2016. Toward an Ediacaran time scale: problems, protocols, and prospects. *Episodes* 39, 540–555. <https://doi.org/10.18814/epiugs/2016/v39i4/103886>.
- Yuan, X., Chen, Z., Xiao, S., Zhou, C., Hua, H., 2011. An early Ediacaran assemblage of macroscopic and morphologically differentiated eukaryotes. *Nature* 470, 390–393. <http://dx.doi.org/10.1038/nature09810>.
- Yuan, X., Chen, Z., Xiao, S., Wan, B., Guan, C., Wang, W., Zhou, C., Hua, H., 2013. The Lantian biota: a new window onto the origin and early evolution of multicellular organisms. *Chin. Sci. Bull.* 58, 701–707. <http://dx.doi.org/10.1007/s11434-012-5483-6>.
- Zhou, C., Xiao, S., 2007. Ediacaran $\delta^{13}\text{C}$ chemostratigraphy of South China. *Chem. Geol.* 237, 89–108. <http://dx.doi.org/10.1016/j.chemgeo.2006.06.021>.
- Zhou, C., Guan, C., Cui, H., Ouyang, Q., Wang, W., 2016. Methane-derived authigenic carbonate from the lower Doushantuo Formation of South China: Implications for seawater sulfate concentration and global carbon cycle in the early Ediacaran ocean. *Palaeogeogr. Palaeoclimatol. Palaeoecol.* 461, 145–155. <http://dx.doi.org/10.1016/j.paleo.2016.08.017>.
- Zhu, M., Zhang, J., Yang, A., 2007. Integrated Ediacaran (Sinian) chronostratigraphy of South China. *Palaeogeogr. Palaeoclimatol. Palaeoecol.* 254, 7–61. <http://dx.doi.org/10.1016/j.palaeo.2007.03.025>.
- Zhu, M., Lu, M., Zhang, J., Zhao, F., Li, G., Yang, A., Zhao, X., Zhao, M., 2013. Carbon isotope chemostratigraphy and sedimentary facies evolution of the Ediacaran Doushantuo Formation in western Hubei, South China. *Precambr. Res.* 225, 7–28. <http://dx.doi.org/10.1016/j.precamres.2011.07.019>.
- Zhu, M., Zhuravlev, A.Y., Wood, R.A., Zhao, F., Sukhov, S.S., 2017. A deep root for the Cambrian explosion: Implications of new bio- and chemostratigraphy from the Siberian Platform. *Geology* 45, 459–462. <http://dx.doi.org/10.1130/g38865.1>.